

HIGH POWER MILLIMETER WAVELENGTH COHERENT RADIATION
SOURCES(U) DARTMOUTH COLL HANOVER N H DEPT OF PHYSICS
AND ASTRONOMY J E WALSH 15 JUN 84 AFOSR-TR-84-0636
AFOSR-82-0168 E/G 20/5

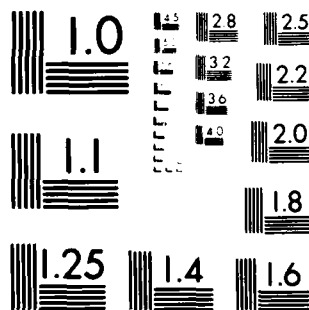
NL

AFOSR-82-0168

F/G 20/5

NL

END
DATE
FILMED
9-84
DTIC



MICROCOPY RESOLUTION TEST CHART
NATIONAL BUREAU OF STANDARDS-1963-A

1a. REPORT SECURITY CLASSIFICATION		1b. RESTRICTIVE MARKINGS	
2a. SECURITY CLASSIFICATION		3. DISTRIBUTION/AVAILABILITY OF REPORT	
2b. DECLASSIFICATION		Approved for distribution	
4. PERFORMING ORGANIZATION REPORT NUMBER(S)		5. MONITORING ORGANIZATION REPORT NUMBER(S)	
6a. NAME OF PERFORMING ORGANIZATION		7a. NAME OF MONITORING ORGANIZATION	
6b. OFFICE SYMBOL (If applicable)		7b. ADDRESS (City, State and ZIP Code)	
6c. ADDRESS (City, State and ZIP Code)		8a. NAME OF FUNDING/SPONSORING ORGANIZATION	
8b. OFFICE SYMBOL (If applicable)		9. PROCUREMENT INSTRUMENT IDENTIFICATION NUMBER	
8c. ADDRESS (City, State and ZIP Code)		10. SOURCE OF FUNDING NOS.	
11. TITLE (Include Security Classification)		PROJECT NO.	
12. PERSONAL AUTHOR(S)		TASK NO.	
13a. TYPE OF REPORT		13b. TIME COVERED	
14. DATE OF REPORT (Yr., Mo., Day)		15. PAGE COUNT	
16. SUPPLEMENTARY NOTATION			
17. COSATI CODES		18. SUBJECT TERMS (Continue on reverse if necessary and identify by block number)	
19. ABSTRACT (Continue on reverse if necessary and identify by block number)		20. DISTRIBUTION/AVAILABILITY OF ABSTRACT	
21. ABSTRACT SECURITY CLASSIFICATION		22a. NAME OF RESPONSIBLE INDIVIDUAL	
22b. TELEPHONE NUMBER (Include Area Code)		22c. OFFICE SYMBOL	

AD-A144 481

N/A

AFOSR-TR.

16

/Research
Air Force Office of ScientificDepartment of the Air Force
Bolling Air Force Base, D.C. 20332

AFOSR-82-0168

PROGRAM
ELEMENT NO.PROJECT
NO.TASK
NO.WORK UNIT
NO.

61102F

2301-A8

High Power Milli-
meter Wavelength Coherent Radiation Sources

John Walsh

Scientific

FROM 2/1/83 TO 1/31/84

6/15/84

79

COSATI CODES

FIELD GROUP SUB. GR.

High power mm-wavelength sources; Cerenkov Maser
oscillators and amplifiers; open resonator
Cerenkov lasers

During the reporting period, Cerenkov Maser resonators with a rectangular configuration were analyzed, constructed and experimentally tested. All of the previous work was based upon cylindrical resonators, a choice which was convenient because of the intrinsic symmetry of the beam transport and focussing. The dominant modes in this case are TM_{0n} . In many potential applications, however, an amplifier would be more useful than an oscillator and a structure which, coupled to a linearly-polarized field, would then be far more convenient. It was for this purpose that the rectangular dielectric slab waveguide structures were analyzed and tested.

The mode structure is designated by LSE and LSM (Longitudinal Section Electric, Magnetic). Both of these couple axially to the electron beam but the LSM mode, which resembles closely a TM mode, has a much greater coupling

DISTRIBUTION/AVAILABILITY OF ABSTRACT

UNCLASSIFIED/UNLIMITED ☐ SAME AS RPT. ☒ DTIC USERS ☐

ABSTRACT SECURITY CLASSIFICATION

Unclassified

NAME OF RESPONSIBLE INDIVIDUAL

Robert Barker

TELEPHONE NUMBER
(Include Area Code)

(202) 767-4907

OFFICE SYMBOL

NP

84 08 17 069

DTIC FILE COPY

strength than the LSE mode.

Numerical codes for plotting the dispersion relations of partially-filled rectangular waveguides and dielectric slab-loaded open rectangular resonators were developed. These were examined in detail in the 50-300 GHz range of frequencies and it was shown that good coupling could be obtained with standard waveguide configurations.

Dielectric-loaded WR-42 and WR-28 waveguides were constructed and tested with the 150-200 KV 1-10 A electron beam generator which has been used in the previous Cerenkov Maser experiments. Oscillation was achieved with both systems. The output power levels were modest in comparison with the 100 KW peak levels achieved with cylindrical system but it is felt that this is due in large part to the (as yet) unoptimized rectangular beam transport system. Oscillation has also been achieved with the open rectangular resonators and during the coming contract year, an input coupler will be designed for this structure and its potential as an amplifier will be evaluated.

Standard waveguides loaded with thin dielectric layers on their broad faces were used as the basis for amplifier calculations. It was found that gains in the range 1-1.5 db/cm could, in principle, be obtained from these structures when they were driven by an electron beam with characteristics similar to our present generator. The fractional 3 db band widths are also potentially very large (full waveguide band is typical). Details of these calculations are presented in an attached appendix. (This document is currently being edited and prepared for publication and preliminary copies will be forwarded when they are available). When a suitable driver is located, the amplifier configuration will also be tested.



Abstract Submitted
For the Twenty-fifth Annual Meeting
Division of Plasma Physics
November 7 to 11, 1983

Category Number and Subject 4.9 Coherent Radiation Generation

☐ Theory

☒ Experiment

³ Free Electron Lasers

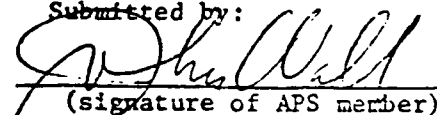
Experimental Performance of a Cerenkov Maser at Lower mm Wavelengths. J. WALSH, E. GARATE, T. BULLER, R.W. LAYMAN, R. COOK and D. WILLEY, Dartmouth College*--Cerenkov Masers have achieved hundred-KW power levels in the middle-mm range and outputs in excess of ten KW in the lower-mm region¹. Substantial output levels, on higher order cavity modes, have also been obtained at wavelengths below 1 mm. However, the typical single-stage high power output pulse is often considerably less than the electron beam pulse length. In the longer wavelength range, two-stage, oscillator-amplifier operation has been used to increase the pulse length and the overall stability of the output. The results of attempts to extend this concept to shorter wavelength will be discussed. In addition, resonator design criteria for fundamental mode operation in the 1-mm wavelength range and preliminary experimental results will be presented.

1. A High Power Cerenkov Maser Oscillator, S. Von Laven et al., Appl. Phys. Lett. 41(5), 408 (1982).

*Supported in part by AFOSR Contract # 82-0168 and ARO Contract # DAAG29-83-K-0018.

- ☐ Prefer Poster Session
☐ Prefer Oral Session
☒ No Preference
☐ Special Requests for placement of this abstract:
☐ Special Facilities Requested (e.g., movie projector)

Submitted by:


(signature of APS member)

John E. Walsh

(same name typewritten)

Physics Department, Dartmouth

(address) College,
Hanover, N.H.

This form, or a reasonable facsimile, plus Two Xerox Copies must be received
NO LATER THAN Noon, Friday, July 15, 1983, at the following address:

03755

Division of Plasma Physics Annual Meeting
c/o Ms. Barbara Sarfaty
Princeton Plasma Physics Laboratory
P. O. Box 451
Princeton, New Jersey 08542

Approved for
distribution unlimited.

84 08 17 069

Abstract Submitted
For the Twenty-fifth Annual Meeting
Division of Plasma Physics
November 7 to 11, 1983

Category Number and Subject 4.9 Coherent Radiation Generation

☒ Theory ☐ Experiment

Excitation of the Slow Cyclotron Wave by the
Passage of a Superluminous Electron Beam Near a
Dielectric Slab*, WILLIAM B. CASE and ROBERT D. KAPLAN,
Grinnell College, and JOHN E. WALSH, Dartmouth College.
We consider the excitation of the slow cyclotron wave
due to the interaction of a superluminous electron
beam passing near a dielectric slab. The analysis is
carried out by treating the electron beam as a cold
fluid which perturbs the degenerate polarization modes
of the electromagnetic waves in free space. The
resulting modes are then matched to the modes within
the dielectric producing a dispersion relation for the
system. When solved using numerical techniques, we
find exponential growths for the slow cyclotron mode
(Cyclotron-Cerenkov) as well as the usual slow space
charge mode (Space Charge-Cerenkov). If this system is
to be used for generation of submillimeter waves, one
must use high γ ($\gamma > 2\pi$) to guarantee good coupling.
In this regime the growth rate for the Cyclotron-
Cerenkov instability is greater than that for the
Space Charge-Cerenkov. Considerations of the effects
of thermal spread will also be given.

*Work supported in part by AFOSR Contract # 82-6108.

- ☒ Prefer Poster Session
☐ Prefer Oral Session
☐ No Preference
☐ Special Requests for placement
of this abstract:
☐ Special Facilities Requested
(e.g., movie projector)

Submitted by:

William B. Case
(signature of APS member)

William B. Case

(same name typewritten)

Grinnell College, Grinnell, Iowa

(address)

50112

This form, or a reasonable facsimile, plus *Two Xerox Copies* must be received
NO LATER THAN Noon, Friday, July 15, 1983, at the following address:

Division of Plasma Physics Annual Meeting
c/o Ms. Barbara Sarfaty
Princeton Plasma Physics Laboratory
P. O. Box 451
Princeton, New Jersey 08544

APPENDIX TO SCIENTIFIC REPORT

CERENKOV MASER AMPLIFIERS

by

John Branscum

Department of Physics and Astronomy

Dartmouth College

Hanover, N.H. 03755

* * *

June 1984

AIR FORCE

Chief, Technical Division

Chapter 1: Introduction

Review of Radiation Sources

Because of potential application in radar and communications, since the 1940's there has been a great amount of interest in producing radiation ranging in wavelength from 30 cm. down to infrared wavelengths of 1 to 10 microns. Two types of sources have filled in much of this part of the electromagnetic spectrum. Traditional microwave sources, such as the klystron, the magnetron, and the traveling wave tube, are capable of producing very high-power radiation down to wavelengths of about 1 cm. They are, however, ultimately limited by the fact that they must contain some sort of resonating structure that is on the order of the wavelength of the produced radiation in size. Thus, as shorter wavelengths and high power are asked for from these devices, several problems, such as tolerances in manufacturing, heat dissipation, and electron-beam focusing become harder and harder to overcome and eventually become insurmountable. The limit of this technology is radiation of wavelengths of about 1mm with power levels in the 100's of watts.

In the infrared part of the radiation spectrum, lasers are very effective sources. They will produce high power radiation at any wavelength for which a molecule with the

desired energy difference in electron orbital energy levels can be found. This is, however, also lasers' major shortcoming; they will not work at any given wavelength, but only those for which such a molecule can be found. Thus they have not been able to fill up the wavelength spectrum smoothly, but rather fill it with randomly placed lines of producible radiation. Therefore, the spectrum of lasers and traditional microwave sources looks something like that shown in Fig. 1-1, with smooth filling but diminishing power down to 1 mm., and then with spotty filling down to optical wavelengths.¹

Free Electron Lasers. the Cerenkov FEL

In the last ten years, the desire to fill the gap between 1 cm. and 10 microns, and to smooth in the spotty coverage below 10 microns, has generated a high level of interest in another type of source, the free-electron laser or FEL. There are several types of FELs, but they all have one thing in common, they are all powered by a high energy electron beam. In general, an FEL will consist of such a beam, plus some sort of interacting structure which can couple energy out of the beam and into an electromagnetic wave. FEL's have the advantage over lasers in that they are in principle continuously tunable over any wavelength, and they have the advantage over traditional microwave

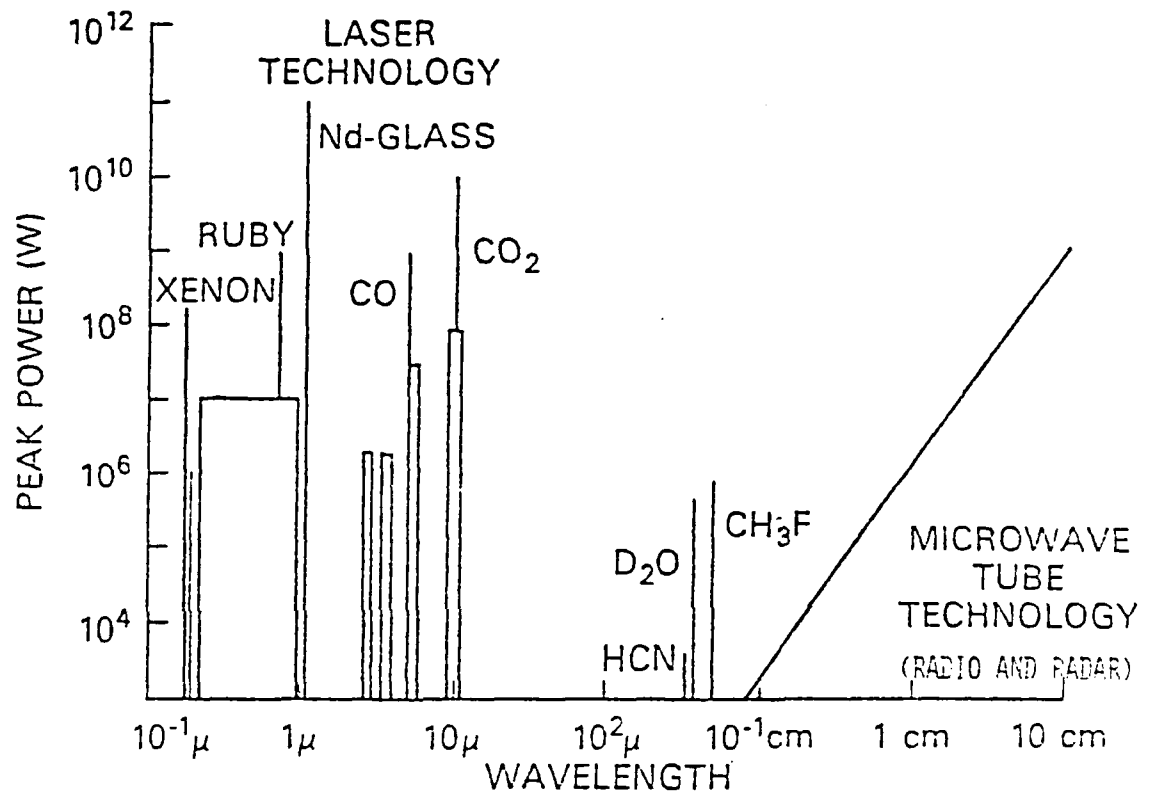


Fig. 1-1. Present-day sources of electromagnetic radiation.

technology in that the FEL's dimensions can be many times larger than the wavelength of the radiation. Exactly how these two advantages are realized is peculiar to each type of FEL, and a survey of the mechanisms is beyond the scope of this paper. We will, however, take a look at the Cerenkov FEL, since it is the type of FEL with which this paper is concerned.

In a Cerenkov FEL the mechanism for coupling energy out of the electron beam is an interaction between the beam and a dielectric. This interaction depends on the fact that the electrons in the beam can be made to travel at velocities greater than the speed of light in the dielectric. It was shown around the turn of the century that any charged particle traveling at superluminal velocities would radiate, sending out an electromagnetic shock-wave similar to the bow-wave of a boat traveling over water at a speed greater than the speed of surface water-waves.² This electromagnetic shock-wave, known as Cerenkov radiation, is the source of radiation in the Cerenkov FEL. The electron beam, traveling at a speed greater than light in the dielectric, is propagated down a waveguide partially filled with dielectric. By keeping the beam close to it, the dielectric is "tricked" into thinking that there actually is a superluminal-velocity particle traveling through it, and Cerenkov radiation is emitted.

Now, for Cerenkov radiation in an infinite medium, all frequencies for which the velocity of the particle is greater than the phase velocity of the wave in the medium are emitted.³ Therefore, in the Cerenkov FEL an infinite number of frequencies will be emitted due to Cerenkov radiation when the beam first enters the guide. However, since the radiation is emitted in the waveguide, and since each frequency emitted will travel down the guide at a discrete phase velocity, there will be a single or a few frequencies that will travel with a phase velocity equal to the velocity of the electron beam. The waves corresponding to these frequencies will therefore travel down the guide along with the beam, and there will be the possibility for prolonged interaction between the beam and these waves. At this point the Cerenkov FEL begins to operate exactly like a conventional traveling-wave-tube. The dielectrically-loaded waveguide acts as a slow-wave structure, and the electron beam, under proper conditions, can be made to do work on the wave, so that there will be growth in the wave at the expense of the energy of the beam. (Fig. 1-2).

It is on this aspect of the Cerenkov FEL that we will focus on in this paper. We will look at one particular resonator geometry, the partially-filled rectangular waveguide, and how it will work as a resonator for a Cerenkov-type FEL/traveling-wave-tube. Therefore our approach will be to assume that a wave already exists in the

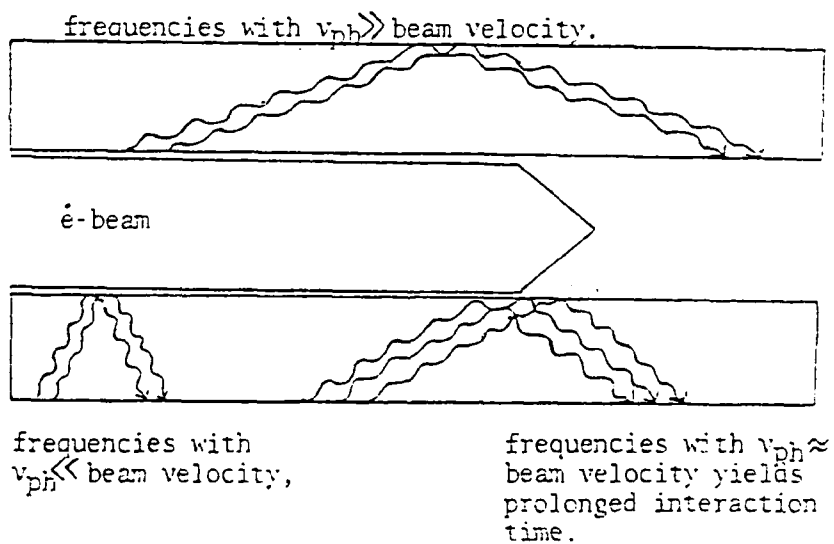
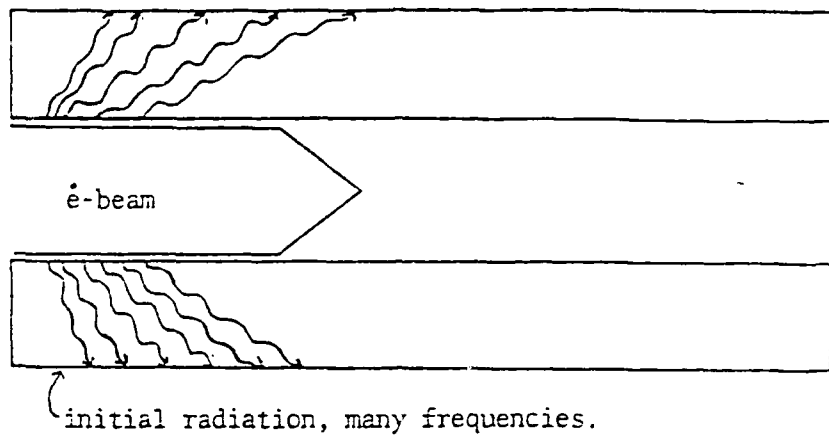


Fig. 1-2. v_{ph} matching of wave with electron beam for discrete frequencies.

guide, and then to introduce an electron beam and allow it to do work on the wave, causing the wave to grow. The Cerenkov interaction is not presented explicitly in the calculations, but it should be kept in mind that this is where the wave originated.

Finally, we refer back to the original statement that the Cerenkov FEL will be useful in filling the gaps left by lasers and conventional microwave technology in the electromagnetic spectrum. Considering tunability, from the above general discussion it can be seen that in principle at least, the Cerenkov device will be tunable simply by varying the beam velocity, so that the beam will be synchronous with waves with different frequencies. (Note that this is a general feature of all traveling-wave-tubes. Note also that the growth rate of the wave will certainly vary as the phase velocity changes, so that the operational bandwidth of the device will also be of concern.) Concerning the problem of the size of the resonating structures, it has been found that in general for a Cerenkov FEL there is a correlation between the resonator dimensions and the output radiation, but that the scaling is such so that the problems mentioned above: heat dissipation, manufacturing tolerances, and beam focusing, are at least partially eased.^{4,5} In this paper we will consider both the bandwidth and frequency output for the partially-filled rectangular resonator for the Cerenkov FEL.

The CERENKOV FEL AT DARTMOUTH COLLEGE

The Cerenkov-type FEL at Dartmouth College has been in operation since 1979. The initial work done with the device focused primarily on determining what the relation was between the voltage of the electron beam and the frequency of the output radiation, and comparing the experimental results with the theoretical predictions discussed above. More recent work has focused on predicting and measuring the output power of the device. Also, while the original output wavelengths were usually between 1 cm and .5 cm, some recent work has centered on trying to get output wavelengths down to the 1mm range.

All of this work has had one thing in common, it has been done using a cylindrical geometry for the resonator design. The cylinder was the initial geometry choice because of its very high level of symmetry, which allowed for the use of the simplest possible electron beam generation and focusing, the simplest schemes for coupling the output radiation out of the device, and also the simplest methods for actually building the parts of the machine.

Motivation for Considering the Rectangular Geometry

While the cylindrical geometry offers several advantages due to its high level of symmetry, it does have two potential disadvantages. The first is a problem that

almost certainly has already been seen with operation of the device at Dartmouth. This is the problem of electron trapping on the inner surface of the dielectric. Inevitably when a high current electron beam is fired down a long tube, some of the beam will strike the inner surface of the tube. Since in the partially-filled, dielectrically-loaded cylinder this inner surface is a dielectric, and in fact, for highest efficiency in operation of the FEL, a very low-loss dielectric, these electrons may have a very difficult time escaping from the dielectric surface and getting to ground. Since it is easier for charge to flow along the surface of a lossless dielectric than through it, the RC time related to the leaking off of these electrons from the dielectric surface will depend on the length of the surface path to ground. This path can be very long in the cylindrical geometry, on the order of the length of the resonator.

In the partially-filled rectangular geometry which we will consider here, however, the surface path length to ground will be on the order of the width of the guide. (Fig. 1-3). Thus we would expect this rectangular resonator to have less of a problem with charge build-up on the dielectric surface. This should allow for more stable beam propagation (the trapped electrons tend to repel the electron beam, which causes problems in getting the beam down the tube), and for generally cleaner operation of the

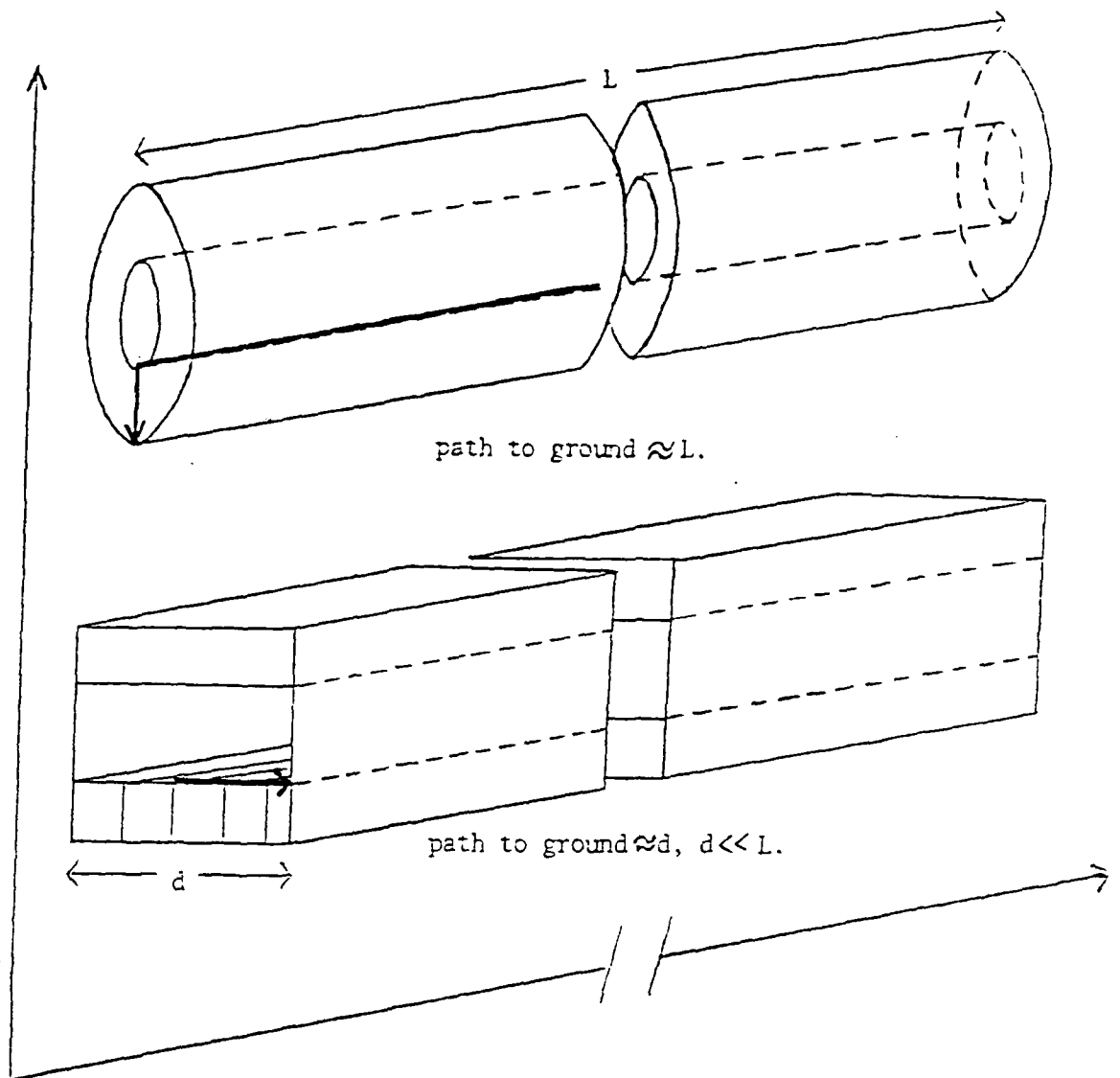


Fig. 1-3. Surface path to ground for cylindrical and rectangular resonators. Path length $l \approx L$ for cylinder, and $l \approx d$ for rectangle. Note $L \gg d$.

device (no breakdown of the dielectric due to excessive charge build-up.)

The second potential disadvantage to the cylindrical geometry is the same high level of symmetry that was initially considered to be of such advantage. This high symmetry makes the control and characterization of the polarization of the output radiation difficult. While polarization of output radiation has not yet been important to this particular experiment, eventual use of the Cerenkov FEL as an amplifier will almost certainly make it so. (We will take a brief look at the potential of a Cerenkov device using the rectangular geometry as an amplifier in chapter 5.) So for these two reasons: charge build-up and control of the polarization of the radiation, we will consider the use of the rectangular geometry as a resonator for use in a Cerenkov-type FEL.

TOPICS

In Chapter 2 we will briefly describe two types of gain calculations which we hope to apply to this geometry, the single-particle and the collective gain calculations. The two types correspond to two regimes of beam density and gain magnitude. The single-particle calculation may be used when the beam density is low and the gain is small, and the collective gain calculation must be used for dense beams and high gains.

In Chapter 3 we will consider the resonator itself in detail and discuss the types of modes that can be propagated in it. We will then present the dispersion relations (from which phase velocity vs frequency information can be obtained) for each of the mode types. The last part of Chapter 3 will look at the actual fields of each mode type and predict the relative growth rates for each. All of the results in Chapter 3 will have been obtained from exact solutions of Maxwell's equations, but details of the calculations will be deferred until appendix 1.

In Chapter 4 we will apply the two gain calculations to the results from Chapter 3, and compare the results. Finally, in Chapter 5 we will consider the use of the rectangular geometry as a high gain, high energy amplifier.

Chapter 2: Gain Mechanisms

Introduction

In this chapter we will discuss two types of gain calculations, the single-particle gain and the collective gain calculations, which we will eventually apply to the rectangular-waveguide resonator geometry. Before getting into specifics, however, let us first consider the general requirements that must be met in order to get significant growth of an electromagnetic wave due to an electron beam doing work on it. First, the electromagnetic wave must have a field component on which the beam can do work, which means a component in the direction of beam travel. (We will now assume that this direction is the z-direction.) Second, the beam velocity should be just greater than the phase velocity of the wave.⁶ This second point is important because if the beam travels at a speed radically different from that of the wave, it will be in the correct phase relation to the wave for too short a time to do any useful work on the wave, and if it travels at a velocity close to the wave velocity, but slightly less than it, the wave will end up doing work on the beam, so that instead of the desired growth of the wave at the expense of beam energy, we would get an acceleration of the beam at the expense of the energy of the wave.

A highly simplified way of looking at this process is to imagine the electrons traveling along with the wave.

where the wave is represented by a series of field-strength peaks and troughs (Fig. 2-1). If the electrons travel at a speed slightly greater than the wave velocity, more electrons will be trying to "run up" the hills, losing energy to the wave, than will be "running down" the hills, and gaining energy from the wave. If however, the beam velocity is less than the wave velocity, the situation is reversed, and more electrons run down the hills than run up them, and the wave loses energy to the beam as it accelerates the beam.

Beam-wave Coupling Strength

An important aspect of the interaction between the beam and the wave is the relative strength of the E_z -component of the wave. Since this is the field component that the electron beam does work against, the stronger this component is relative to the other components of the wave, the more powerful the interaction between the beam and wave will be. This fact will be shown to be very important in chapters 3 and 4.

Single-Particle Gain Calculation

In this calculation the general approach is to first use Maxwell's Equations to determine the fields in the resonator. Then, while keeping these fields constant, the electron beam is introduced, and each electron in the beam

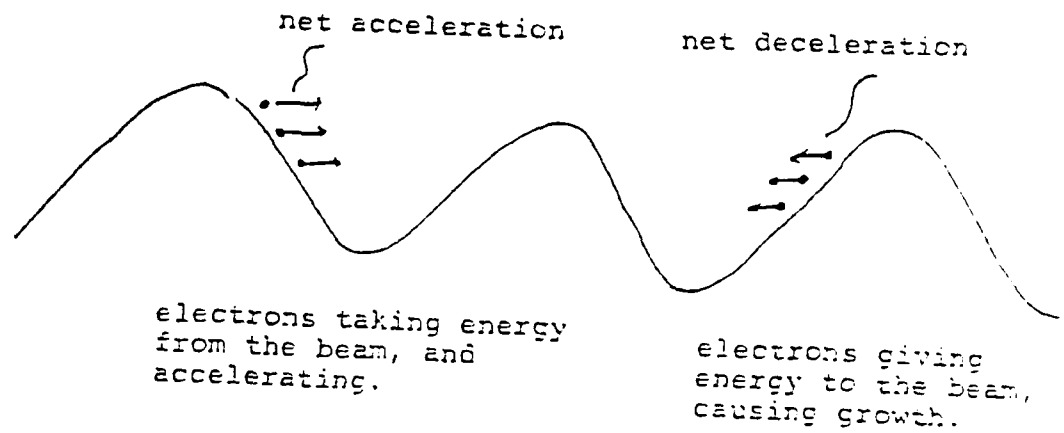


Fig. 2-1. Electron - Wave interaction: "Hill and Trough" model.

is allowed to do work on the fields in the resonator. No account is taken of how the other electrons in the beam may affect this interaction of a single electron with the fields, and no account is taken of how the fields may change due to the work being done on them by the electrons. Therefore this calculation is most useful when the beam is tenuous enough so that the electron-electron interactions may be ignored, and when the gain is small enough so that the fields may be approximated as being constant during the transit time of an electron in the beam through the resonator. Since the calculation has already been well presented,⁷ only the initial assumptions, the results, and a few comments will be presented here.

We first note that any growth rate (or loss rate) may be expressed as an inverse cavity Q , where:

$$\frac{1}{Q_b} = \frac{-1}{\omega \mathcal{E}} \frac{d\mathcal{E}}{dt}$$

and where:

Q_b = cavity Q due to the beam,

\mathcal{E} = the total energy stored in the resonator, and

ω = the frequency of the radiation in radians.

Therefore, $1/Q_b$ is a relative measure of energy gained or lost in one period by the wave.

There is one important assumption other than the low beam density made in doing this calculation. This

assumption is that the beam is relatively cold, (i.e. that most of the electrons are traveling at the same velocity.) so that we may approximate the electron velocity distribution as a delta function in velocity space. With this assumption, the single-particle gain calculation yields:

$$\frac{1}{Q_b} = \frac{1}{\beta^3 \gamma^3} \frac{I_b}{I_0} \frac{n}{n_0} \frac{L^3 E_{z0}^2}{8\epsilon} G'(e)$$

where: $\beta = \frac{v_{ph}}{c}; \quad \gamma = \frac{1}{\sqrt{1 - \beta^2}}$

(note that we have assumed that v_{phase} of the wave $\approx v_{beam}$)

and where:

I_b = beam current

$$I_0 = \frac{ec}{r_0}, \text{ where } r_0 = \frac{e^2}{mc^2}, (I_0 \approx 17,000 \text{ amps}).$$

also, L = resonator length,

E_{z0} = a field amplitude at some reference point.

\bar{n} = a relative beam density term, which equals

$$\bar{n} = \frac{dA n |E_z|^2}{|E_{z0}|^2 A_b}$$

A_b = beam area

where n = the beam density (a point function,
set equal to n_0).

E_z = the electric field in the direction
of beam propagation.

(also a point function)

and finally, $G(\Theta) = \frac{1}{2} \frac{\sin^2 \Theta}{\Theta^2}$, where $\Theta = (kv - \omega)L/v$.

It is this last term, $G'(\Theta)$, that contains the crucial information concerning whether work will be done by the beam on the wave, or visa versa. It describes the phase slippage that an electron in the beam sees relative to the wave during one pass through the resonator. Put more simply, it tells whether more electrons run up hills or down them. A plot of $G'(\Theta)$ vs. Θ is given in Fig. 2-2. For the beam to do work on the wave, it turns out that $G'(\Theta)$ must be < 0 . We will therefore assume for the rest of the paper that $\Theta = 2.2$, so that $G'(\Theta) = -.13$, which will give us maximum gain as a function of Θ .

Collective Gain Calculation

In this calculation the electron/electron interactions are taken into account by treating the electron beam as a fluid subject to the standard continuity and conservation equations. There are several possible approaches to this problem, but the one used here has been chosen because it is

Line shape vs. theta

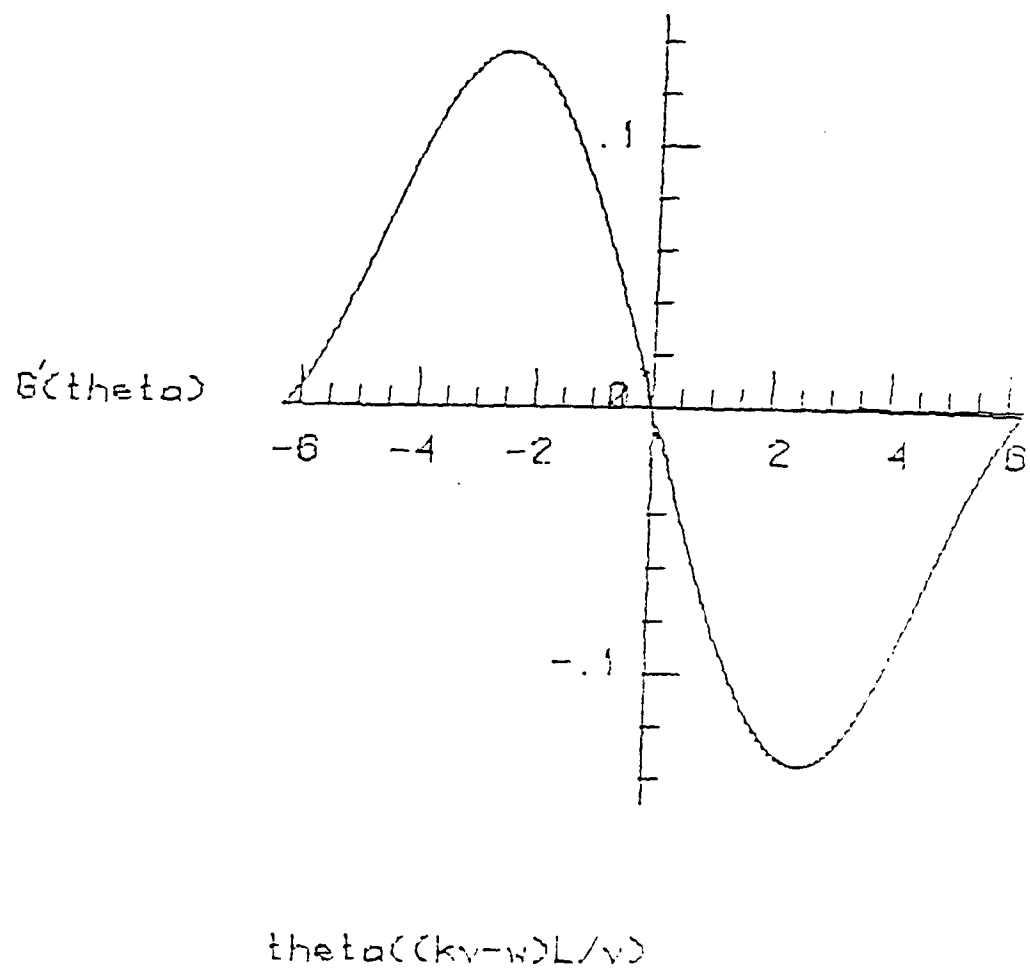


Fig. 2-2. $G(\theta)$ vs. θ , where $\theta = (kv - \omega)L/v$.

a well-known technique with well-known results. It is presented in its entirety by Felch,⁸ so again, only the initial assumptions, the results, and comments are given here.

The approach used by Felch is to first derive the usual dispersion relation for the empty resonator, and then to introduce the electron beam. A second dispersion relation is derived, this time including the beam in Maxwell's Equations. Finally, the beam-dispersion relation is expanded about the no-beam relation, using a Taylor series expansion:

$$D(\omega, k) = D(\omega_0, k_0) - \frac{\partial D}{\partial \omega} \bigg|_{\omega_0, k_0} \Delta \omega$$

where $\Delta \omega$ is the complex frequency shift due to the presence of the beam. The imaginary part of this shift gives the growth-rate of the wave due to the beam. Note that the only assumption made in this calculation is that the expansion given above is valid, which requires simply that $\frac{\Delta \omega}{\omega} \gg 1$. Thus there is no requirement on the beam density or on the total gain, as long as this initial assumption holds.

Since the form of $\Delta \omega$, will depend directly on the form of the dispersion relation, its exact solution is not given until Chapter 4. (The dispersion relation is found in Chapter 3.)

Chapter 3: Fields and Modes for the Rectangular Resonator

LSM and LSE Modes

We will now take a close look at the modes for the partially-filled rectangular resonator. The dimensions of the waveguide are given in Fig. 3-1, and the dielectric constant of the dielectric slabs in the resonator is ϵ . This waveguide geometry will support two different mode-types, called LSE and LSM modes⁹ which are distinguished by the absence of particular field components. In the LSE mode the E_x field component is zero while in the LSM mode the B_x field component is zero. (LSE mode stands for longitudinal section electric mode which means simply that all E fields are parallel to the dielectric interfaces. Similarly LSM mode stands for longitudinal section magnetic mode.) (Fig. 3-2)

Each of the above mode-types LSE and LSM yields a different dispersion relation or frequency vs. phase velocity condition. These two dispersion relations are obtained by first finding the proper field shapes for each mode and then matching the proper boundary conditions across the dielectric interfaces. (See appendix 1 for a complete description of the derivation.) The two dispersion relations so derived are given below.

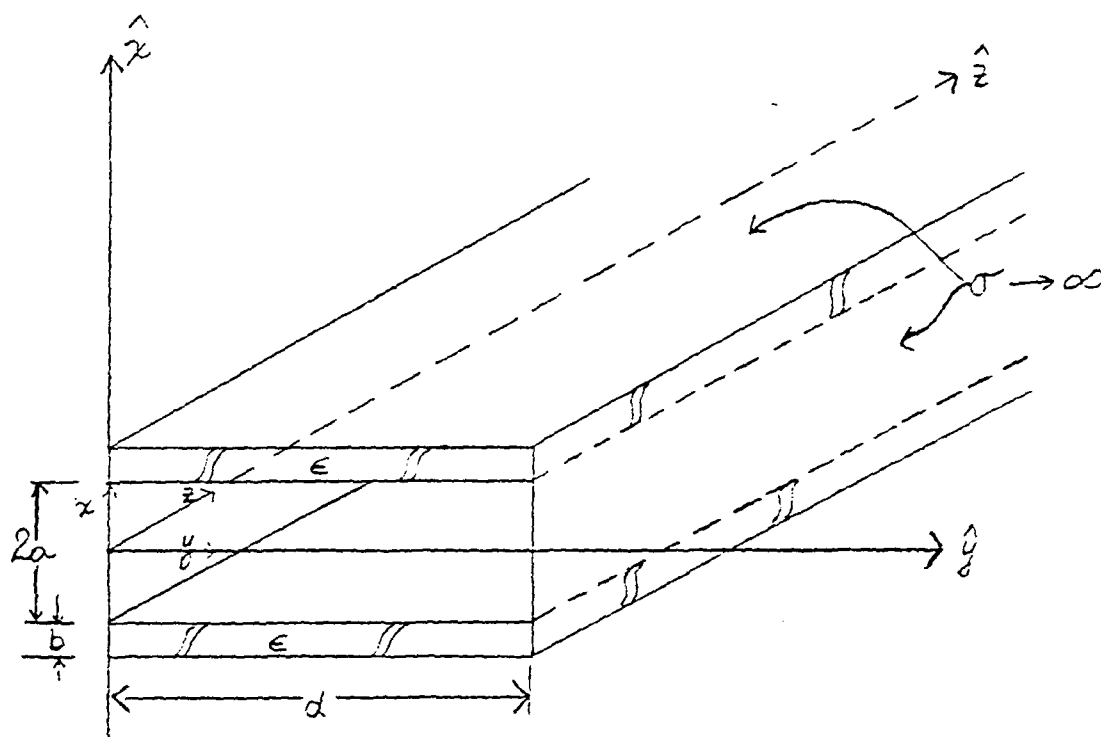
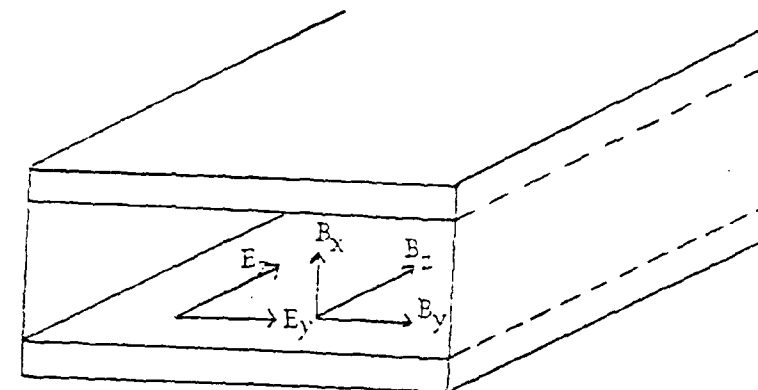
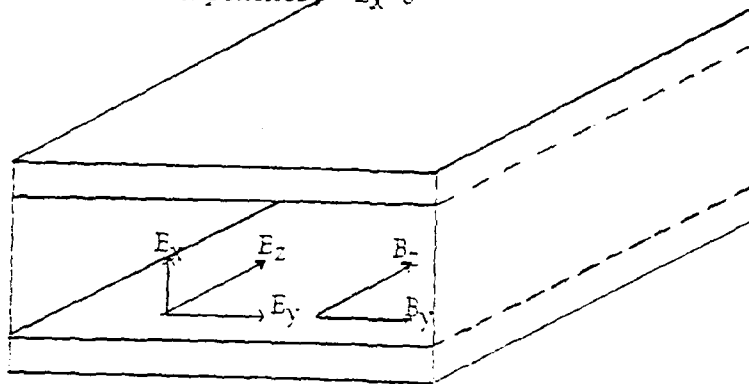


Fig. 3-1. General dimensions of rectangular waveguide with dielectric slabs.



LSE field components, $E_x=0$



LSM field components, $B_x=0$

Fig. 3-2. Field Components of LSE and LSM modes.

$$\text{LSM} \quad \frac{\tanh(qa)}{qa} = \frac{\cot(sb)}{sb} \frac{\epsilon b}{a}$$

$$\text{LSE} \quad (qa) \tanh(qa) = \frac{a}{b} (sb) \cot(sb)$$

$$\text{where} \quad q^2 = k^2 - \frac{\omega^2}{c^2} + t^2 ;$$

$$s^2 = \frac{\omega^2 \epsilon}{c^2} - k^2 + t^2$$

$$\text{and} \quad t = \frac{n\pi}{d} \quad n = 1, 2, 3, \dots$$

and finally where

ω = frequency in radians,

$k = 2\pi / \lambda_g$ and λ_g = the guide wavelength.

The Infinite, Two-slab Resonator; Comparison of LSE and LSM Modes with TE and TM Modes

A highly simplified but similar geometry to the partially filled rectangular waveguide is the infinitely wide, two-slab waveguide. (Fig. 3-3) Solving Maxwell's equations for this resonator reveals that this geometry will support two different mode types and that these mode types are the familiar transverse electric ($E_z = 0$), and

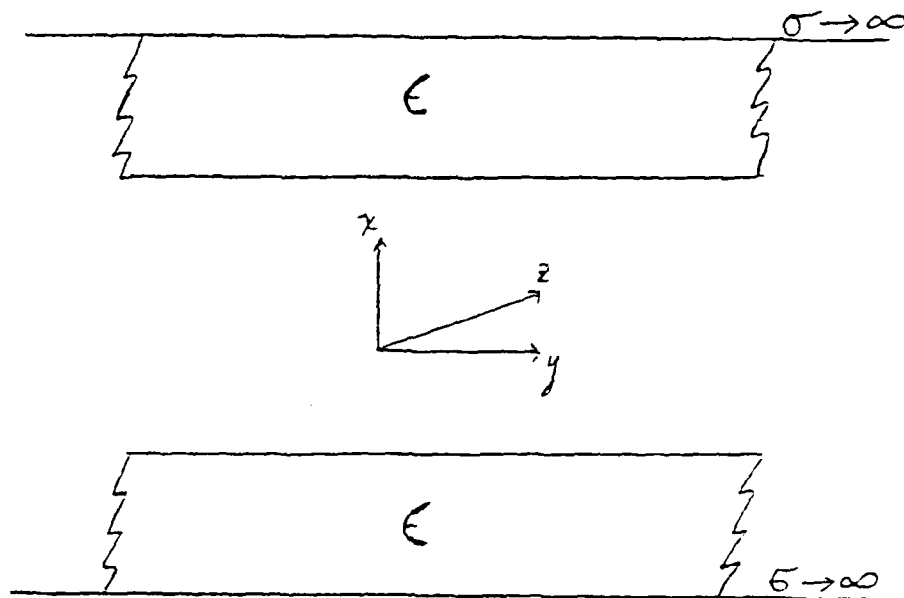


Fig. 3-3. Infinite, 2-slab geometry; (no variation with y).

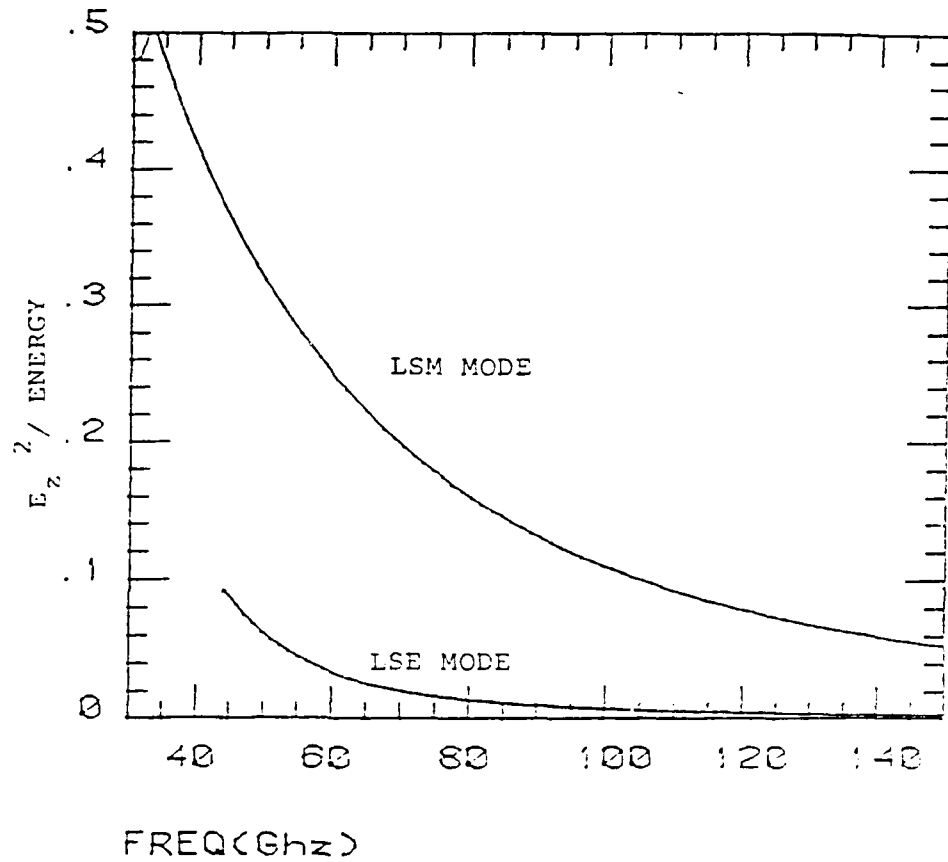
transverse magnetic ($B_z = 0$) modes that are characteristic of many waveguide systems. A close look at the fields of the TE and TM modes reveals a close parallel between them and the LSE and LSM modes. It can be shown that for the TM(E) mode with no variation in the y-direction $B_x(E_x)$ must equal 0. Thus the LSM and TM modes both have $B_x = 0$, and the LSE and TE modes have $E_x = 0$.

We might therefore expect the two sets of modes to share other characteristics. Specifically, since $E_x = 0$ for both the TE mode and the LSE mode, and since $E_z = 0$ for the TE mode, we might expect the LSE mode to have a relatively weak E_z component. If this is found to be true, then as was noted in Chapter 2, the coupling between the electron beam and an LSE wave would also be relatively weak. To test the hypothesis we plot

$$\frac{\text{Energy contained in } E_z \text{ field component}}{\text{Total Energy in the fields in the resonator}}$$

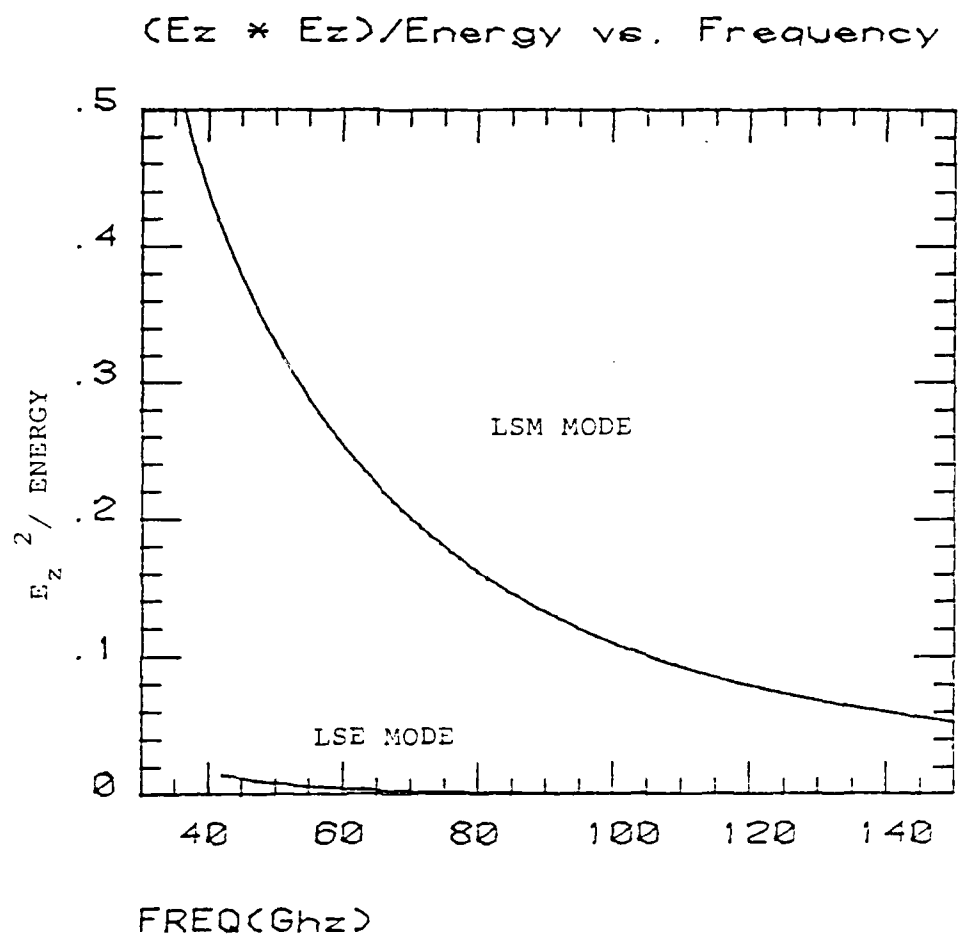
for both the LSE and LSM modes. These plots are shown in Figs. 3-4 & 3-5. In Fig 3-4 the dimensions of the resonator used are typical of what we would expect to use in a real experimental situation. In Fig.3-5 we let the y-dimension of the resonator get very large, to show that the LSE mode does become even more TE-like as the infinite.

$(E_z * E_z) / \text{Energy}$ vs. Frequency



WR-42 Waveguide
Slab thickness = 1mm

Fig. 3-4. (Energy stored in z-component of electric field) / (Total Energy stored) for LSE and LSM modes; for WR-42 waveguide.



WR-42 Waveguide, except width = 30 cm.
Slab thickness = 1mm.

Fig. 3-5. (Energy stored in z-component of electric field)/(Total Energy stored) for LSE and LSM modes, with width of waveguide $\rightarrow \infty$.

2 slab dimensions are approached. As we expected, the relative amount of energy found in the E_z field component of the LSE mode is much less than that for the LSM mode.

In Chapter 4 we will actually calculate the growth rate for both modes, and we will see that this lower E_z strength does indeed give worse beam-wave coupling and lower growth rates for the LSE mode. Therefore, we will defer further discussion of the LSE mode until then and concentrate in the higher growth-rate, and so potentially more useful, LSM mode.

Potential Experimental Parameters: Cerenkov
Millimeter FEL

Up to this point our discussion of the LSE & LSM modes has been very general. Now, however, we choose specific sets of dimensions and parameters for the resonator, where our choices are based on convenience in terms of eventual experimental application in the Dartmouth Cerenkov FEL. Note that even though we lose generality in terms of the actual numbers produced here, the techniques used are applicable to any set of parameters that may be available.

The Dartmouth Cerenkov FEL experiment is a low voltage, low current device that is meant to run in the millimeter and submillimeter part of the radiation spectrum. Since it uses boron nitride as the dielectric in its resonators, we also will do so. (Boron nitride has a dielectric constant

of 4.2). Also, we will limit our voltage range to from 0 to 300 KV, again because this is what is available from the Dartmouth FEL. Finally, for resonator dimensions we choose three commercial waveguide sizes that are commonly used in standard millimeter wave applications. These choices will make building actual resonators to match our theoretical models very easy and inexpensive. The waveguide sizes are labeled WR-42, WR 28, and WR 12, and their dimensions are shown in Fig. 3-6.

LSM-Mode: Output Frequency Characterization

Now that we have chosen a definite set of parameters for our resonator, we are ready to use them in the LSM mode dispersion relation to determine what frequencies we might expect from an actual device using these dimensions. (We will consider frequency output rather than wavelength output because this is what has traditionally been used in the Dartmouth FEL experiment) Therefore we return to this dispersion relation:

$$\frac{\tanh(qa)}{qa} = \frac{\epsilon b}{a} \cot(sb)$$

We plot output frequency ($\nu = \omega / 2 \pi$) vs. operating voltage for several slab thicknesses in each of the

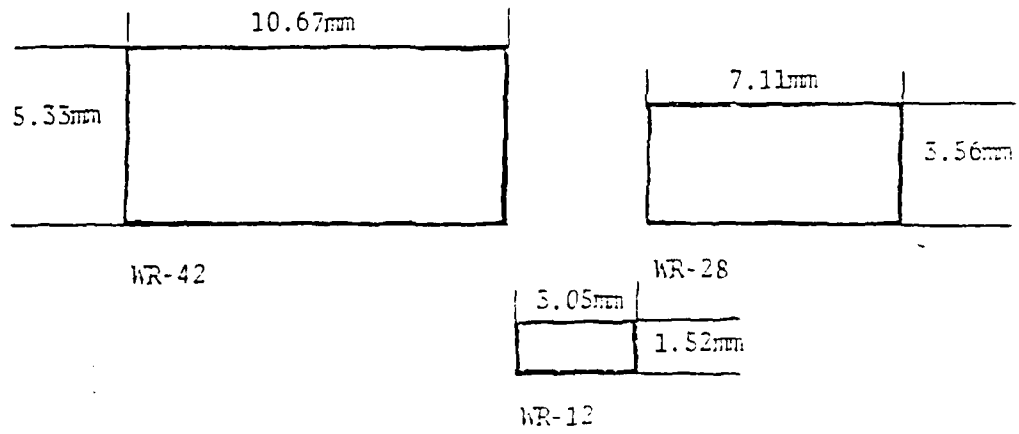


Fig. 3-6. Dimensions for WR-42, WR-28, and WR-12 size waveguides.

waveguide sizes. Again note that operating voltage is determined by matching the phase velocity of the wave with the beam velocity for a given beam voltage. (Figs. 3-7, 8, 9).

Comments

We note immediately that frequency does scale as the dimensions of the resonator, both in terms of guide dimensions and in terms of dielectric slab thickness. Therefore we will eventually run into the same problems mentioned in the introduction, such as heat dissipation and beam focusing, as we try to go to higher frequencies (shorter wavelengths). However, operation at 100 Ghz and above is considered interesting and potentially useful, and note that both the WR-28 and the WR-12 guides can be made to operate in that region of the spectrum. The WR-42 resonator also will operate above 100 Ghz, but only with relatively thin dielectric slabs.

Thus, operation above 100 Ghz is possible with these commercially available waveguide sizes and with moderately thin dielectric liners. Now the gain calculations reviewed in Chapter 2 will be returned to in an attempt to determine whether significant growth rates can be obtained from this geometry at these desired frequencies.

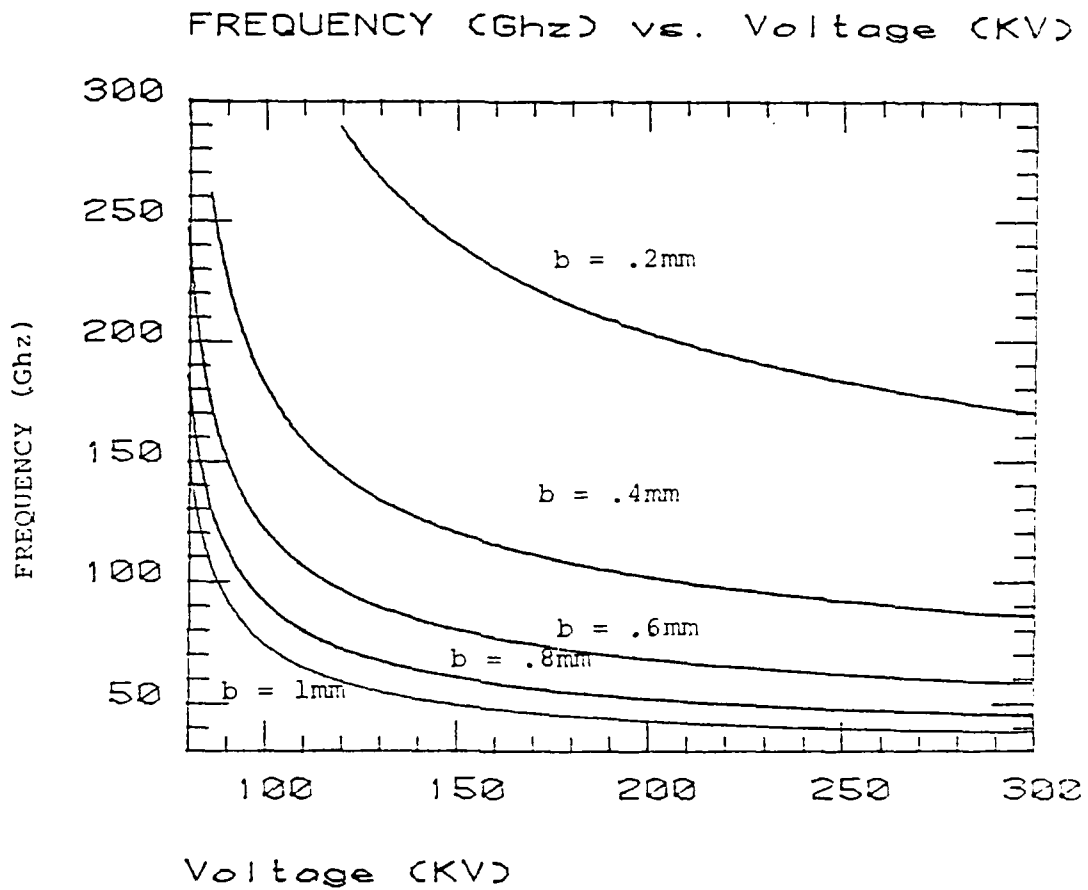


Fig. 3-7. Radiation frequency vs. operating voltage for WR-42 waveguide, with different dielectric slab thicknesses. Dielectric constant = 4.2. (b = slab thickness).

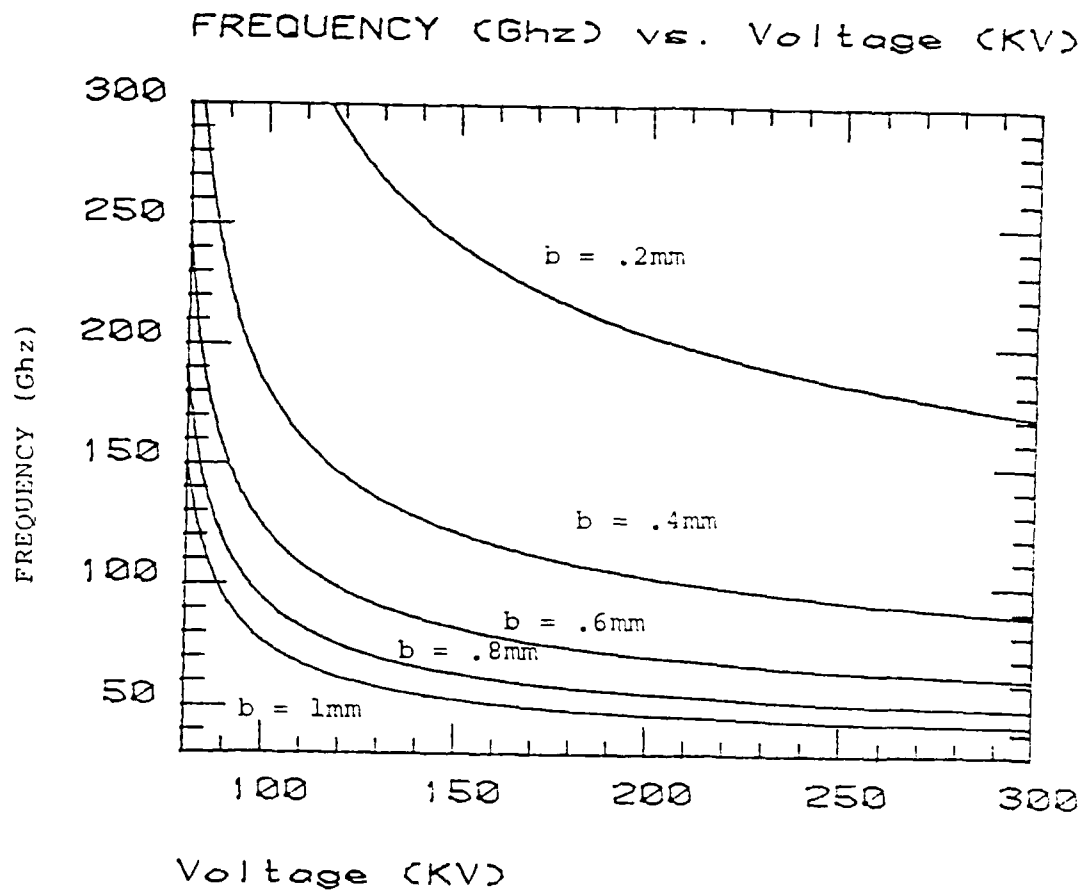


Fig. 3-8. Radiation frequency vs. operating voltage for WR-28 waveguide, with different dielectric slab thicknesses. Dielectric constant = 4.2. (b = slab thickness).

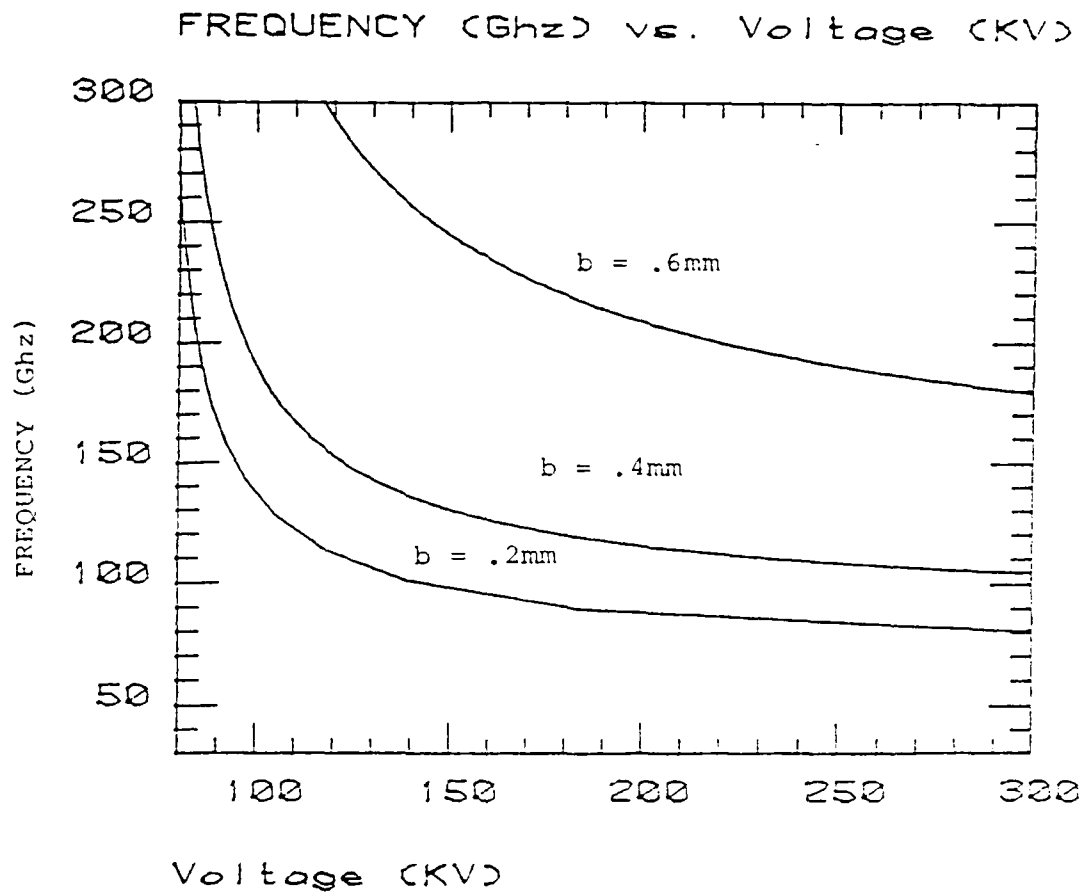


Fig. 3-9. Radiation frequency vs. operating voltage for WR-12 waveguide, with different dielectric slab thicknesses. Dielectric constant = 4.2. (b = slab thickness).

Chapter 4: Gain for the LSE & LSM Modes

Beam-Dielectric Separation: Gain Mechanism Detuning

As noted in Chapter 1, if too many electrons from the electron beam are allowed to strike the dielectric slabs in the resonator, unstable beam propagation, and eventually, damage to the dielectric slabs will result. Even though the rectangular geometry should have better charge bleed-off properties than the cylindrical resonator, no lossless dielectric can tolerate large-scale electron dumping on it for prolonged periods of time. Therefore, in any real device there will have to be some separation of the electrons from the dielectric to prevent too many "stray" electrons from striking the slabs. This separation will, of course, affect the interaction between the electrons and the dielectric, and so will affect the growth-rate of the device. Thus we must account for this separation while doing the single-particle and collective growth-rate calculations. To do this we note the term:

$$\frac{n}{n_0} = \frac{1}{n_0} \frac{\int dA n |E_z|^2}{|E_{z0}|^2 A_b}$$

from the single-particle gain expression in chapter 2. If we let the beam density be constant over the beam area, but have the beam a distance h away from the dielectric, we find that n is given by:

$$\frac{\bar{n}}{n_0} = \frac{1}{4 \cosh^2(qa)} \left[\frac{\sinh[2q(a-h)]}{2q(a-h)} + 1 \right]$$

(see appendix 2)

This expression will be used directly in the single-particle calculation, and gives exactly the effect of the beam-dielectric gap on it.

Unfortunately, there is no direct way to account for the beam-dielectric gap in the collective gain calculation. We can, however, use the single-particle result to get an effective beam current density, which will give us an approximation of the effect of the gap on the growth-rate. To do this we note that if we let $h = 0$, we are effectively allowing the beam to fill the entire vacuum region of the resonator, which is the assumed situation for the collective calculation. For $h = 0$ we get:

$$\frac{\bar{n}_{h=0}}{n_0} = \frac{1}{4 \cosh^2(qa)} \left[\frac{\sinh(2qa)}{2qa} + 1 \right]$$

We can use the ratio of these two expressions to get an effective current density for the beam. We simply take $n_h/n_{h=0}$, and multiply it times the beam current density. Thus we have:

$$\frac{I_{b(\text{eff})}}{2d(a-h)} = \frac{I_b}{2ad} \left[\frac{\left[\frac{\sinh[2q(a-h)]}{2q(a-h)} + 1 \right]}{\left[\frac{\sinh(2qa)}{2qa} + 1 \right]} \right]$$

Using this effective beam current density in the collective calculation will take into account the detuning of the growth-rate due to the presence of the gap.

Finally, a reasonable value for h , with moderate efforts at electron-beam focusing, is $h = .1\text{mm}$.¹⁰ Smaller values of h are in practice achievable, but only with fairly sophisticated electron-focusing techniques. We will therefore use $h = .1\text{mm}$ for the remainder of this paper.

SINGLE PARTICLE GAIN CALCULATION

Now that we have an expression for n/n_0 , we need only an expression for the total energy stored in the resonator to finally get the single-particle $1/Q_b$. The total energy is found by a simple integration of the fields over the resonator (See appendix 3), and the results of this integration, for each of the two mode types, are given below.

$$\epsilon_{LSE} = \frac{dL}{16\pi} |E_{z0}|^2 \left[1 + \frac{k^2}{t^2} \right] \left[b\epsilon [1 + \cot^2(sb)] \right. \\ \left. \left[1 - \frac{\sin(2sb)}{2sb} \right] + \frac{a}{\cosh^2(qa)} \left[1 + \frac{\sinh(2qa)}{2qa} \right] \right]$$

$$\epsilon_{LSM} = \frac{dL}{16\pi} |E_{z0}|^2 \frac{\omega^2}{c^2} \left[1 + \frac{t^2}{k^2} \right] \left[\frac{b^3 \epsilon^2}{(sb)^2} \right. \\ \left. \left[1 + \frac{\sin(2sb)}{2sb} \right] [1 + \cot^2(sb)] + \frac{a^3}{(qa)^2} \frac{1}{\cosh^2(qa)} \left[\frac{\sinh(2qa)}{2qa} - 1 \right] \right]$$

We are now able to compute $1/Q_b$. Note, however, that for amplifiers a more commonly used parameter than the resonator Q_b is the gain per pass, which will be of the form $e^{\alpha L}$. To find αL from $1/Q_b$, we note that if the fields in the resonator have a temporal growth-rate of the form $e^{2\Delta\omega t}$ (the reason for this choice will become clear when the collective calculation is done) we find from its definition, that $1/Q_b$ will be equal to $2\Delta\omega/\omega$, so that the temporal growth-rate will be $e^{(\omega/Q_b)t}$. Now note that the growth per pass will equal the temporal growth-rate with t replaced by τ ,

$\tau = L/v$, the transit time of an electron through the resonator. Therefore we have:

$$\frac{\omega \tau}{Q_b} = \frac{\omega L}{Q_b v} = \propto L$$

Finally, at synchronism (v_{ph} = beam velocity) we have $v = \omega/k$, so that:

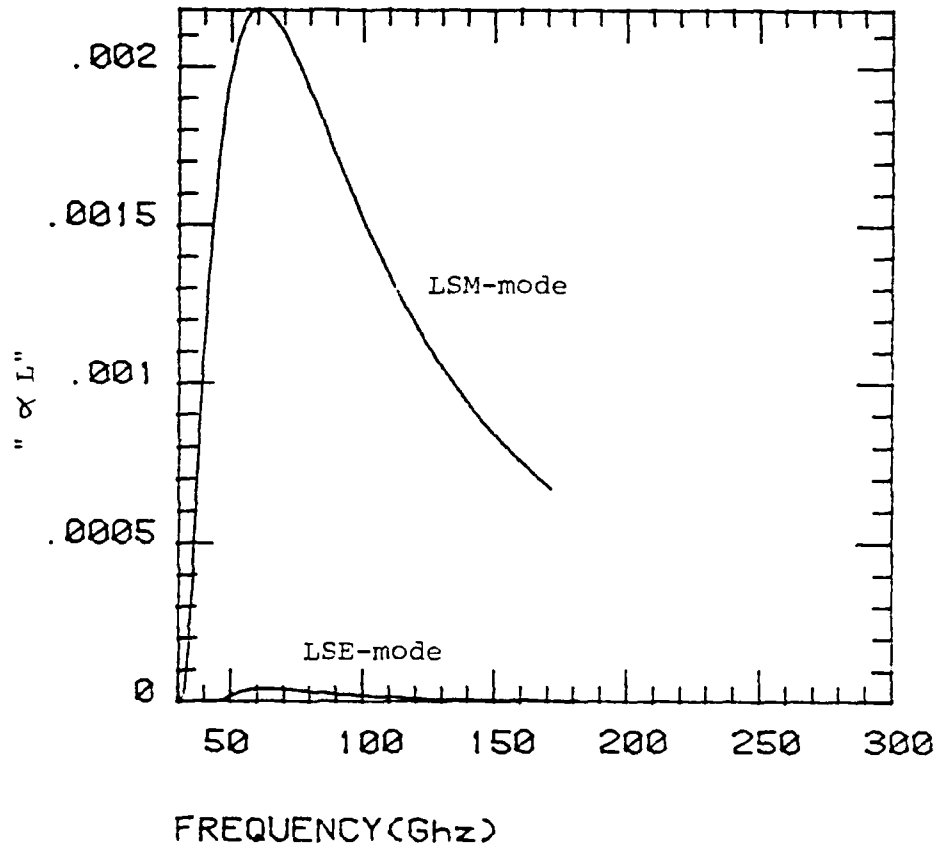
$$\frac{kL}{Q_b} = \propto L$$

Thus we are able to find $\propto L$, which is the parameter we now plot. From the expressions for $1/Q_b$ and the total energy in the resonator it can be seen that the expression for $\propto L$ will have a term $L^3 I_b / I_0$ in the numerator. Therefore we divide out this term and plot finally a current and resonator-length independent quantity: (Fig. 4-1 - 4-4)

$$\frac{\propto L}{\left[\frac{L^3 I_b}{I_0} \right]}$$

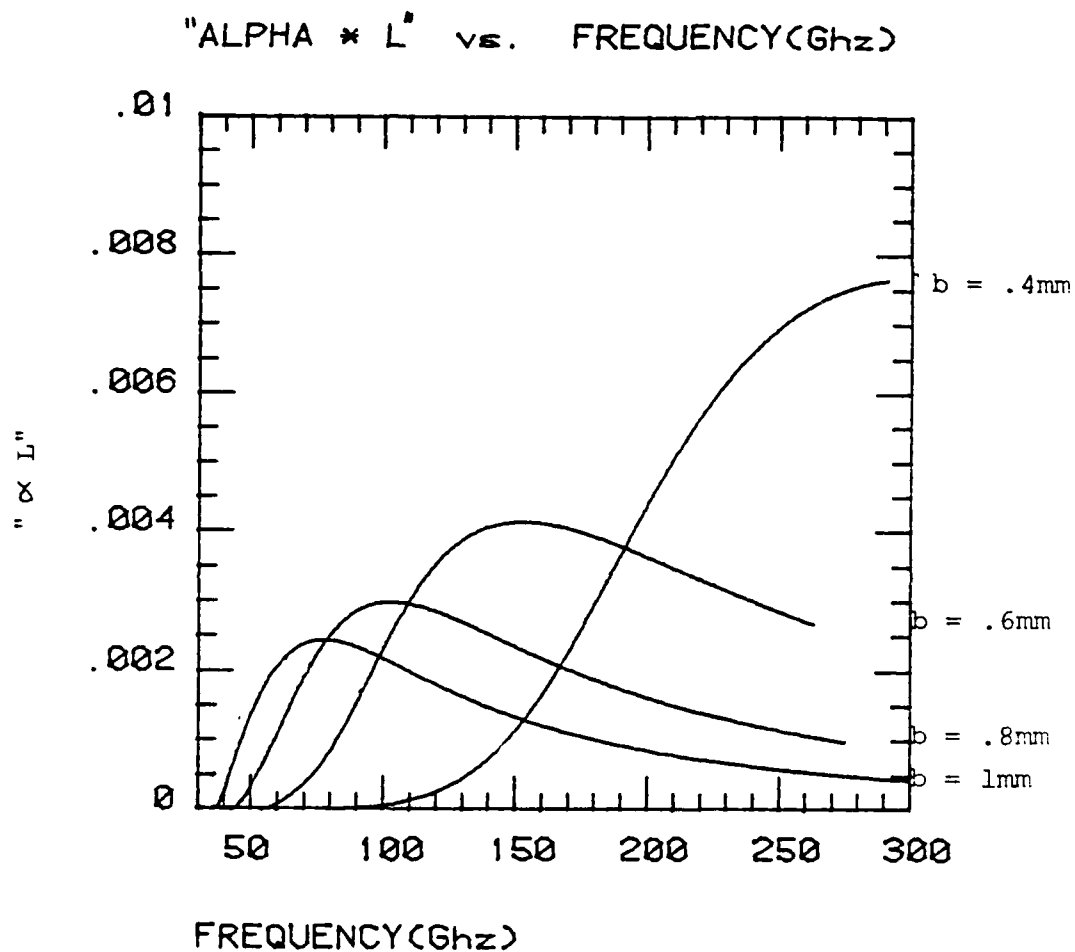
In Fig. 4-1 we have plots for both the LSE and LSM modes using typical potential experimental parameters. We immediately see that $\propto L$ for the LSE mode is in fact much less than for the LSM mode, justifying the previous concentration on the LSM mode. In Fig. 4-2 - 4-4, $\propto L$ for each of the three waveguide sizes is plotted, where for each

"ALPHA * L" vs. FREQUENCY(Ghz)



$$\alpha L = \frac{\alpha L}{\frac{L^3 I_b}{I_0}}, \quad I_0 = 17000 \text{ amps.}$$

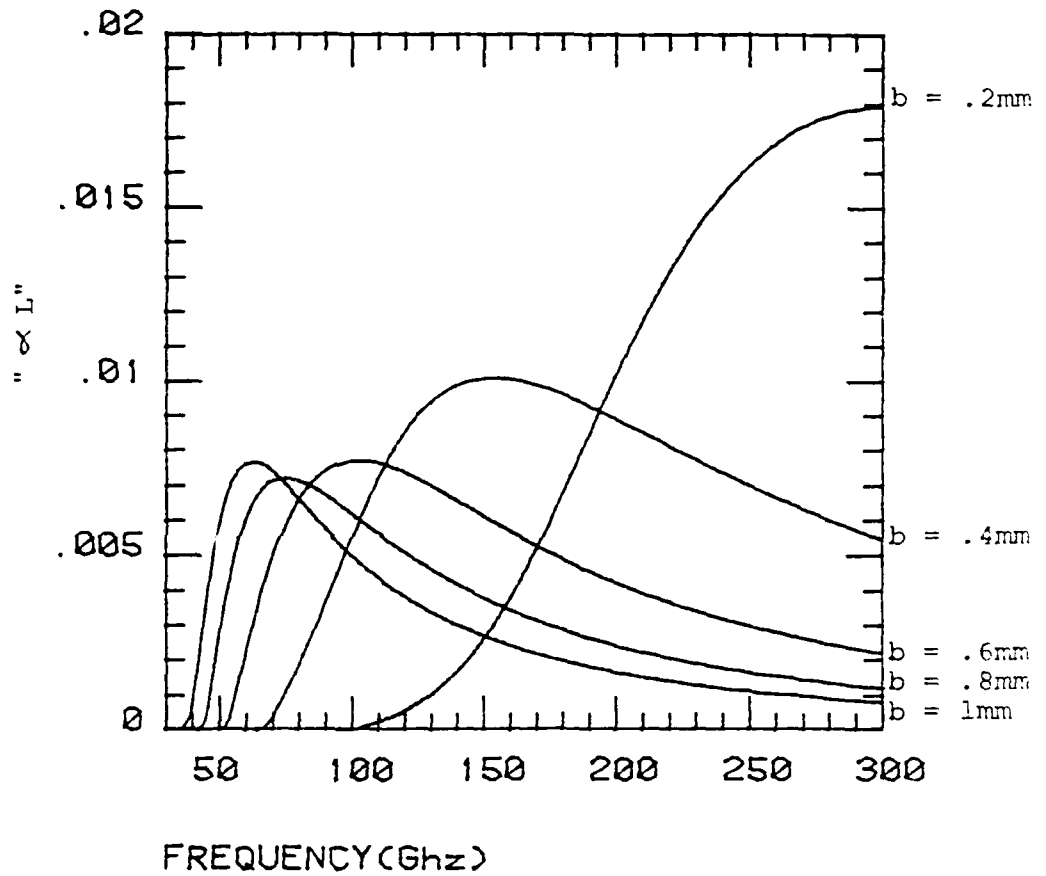
Fig. 4-1. Single-Particle $\alpha L/L^3(I_b/I_0)$ for LSE and LSM modes. Resonator dimensions: WR-42 waveguide size, with 1mm thick dielectric slab.



$$"\alpha L" = \frac{\alpha L}{L^3 \frac{I_b}{I_0}}, \quad I_0 = 17000 \text{ amps}$$

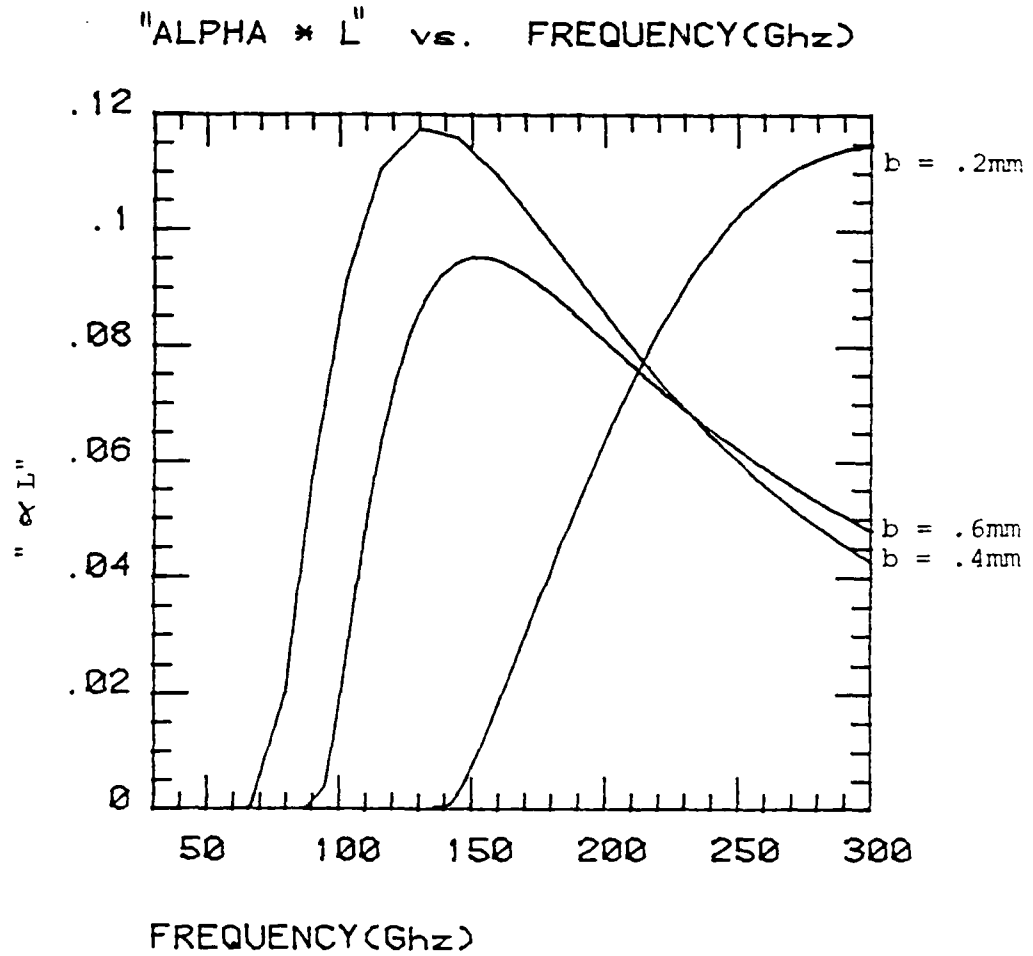
Fig. 4-2. Single-Particle $\alpha L/L^3 (I_b/I_0)$, for WR-42 size resonator. (b = dielectric-slab thickness)

"ALPHA * L" vs. FREQUENCY(GHz)



$$\alpha L = \frac{\alpha L}{\frac{L^3 I_b}{I_0}}, \quad I_0 = 17000 \text{ amps.}$$

Fig. 4-3. Single-Particle $\alpha L/L^3(I_b/I_0)$, for WR-28 size resonator. (b = dielectric-slab thickness).



$$" \alpha L " = \frac{\alpha L}{\frac{L^3 I_b}{I_0}}, \quad I_0 = 17000 \text{ amps.}$$

Fig. 4-4. Single-Particle $\alpha L/L^3(I_b/I_0)$ for WR-12 size resonator. (b = dielectric-slab thickness).

waveguide size, several dielectric-slab thicknesses have been tried.

Single Particle Growth-rate Analysis

One striking result of the growth rate calculation for the different waveguide sizes is the apparent very low gain for the larger waveguides. However, this result is misleading. Remember that the plots shown represent αL divided by beam current, and no account has been made of the smaller waveguide size in relation to this total current. Naturally, the smaller guides will have a higher current density for a given current and so will have higher gains. To get truly equivalent growth-rates for different waveguide sizes, the gain of the larger waveguide should be multiplied by the ratio of the area of its beam region to the area of the beam region of the smaller guide to which it is being compared. If this factor were included, it can be seen that the waveguides would be roughly equivalent in gain.

Operational Wavelength

Two important parameters can be determined from the shape and position of the gain curves in relation to the frequency spectrum. These parameters are the optimum operating frequency, and the frequency bandwidth. Ideally the operating frequency of a promising experimental device should be as high as possible, and it should be at least

greater than or equal to 100 Ghz. We see that any of the waveguide geometries with gain plotted here satisfies that criterion, as long as we restrict the geometry to moderately thin dielectric slab thicknesses of .8 to .6mm. As expected, the WR-12 waveguide gives the highest operating frequencies (smallest wavelengths), but of course will have the most trouble with beam focusing and heat dissipation. Any of these resonators, however, can be made to operate at "interesting" frequencies of 100 Ghz or higher.

Resonator Bandwidth

The second important parameter that can be determined from these plots is the potential operational bandwidth of a device using these resonators. It is obvious from the plots that these resonators offer an enormous band-width. Even the worst case shown, the WR-28 guide with 1mm thick dielectric slabs, offers a half-maximum to half-maximum frequency bandwidth of about 45 Ghz, with a center frequency of 60 Ghz. Such an enormous bandwidth would be very attractive in any type of oscillator or amplifier.

COLLECTIVE GROWTH RATE

As mentioned in Chapter 2, the collective growth-rate can be derived from an expansion of the dispersion relation which includes the beam, about the dispersion relation which does not include the beam. The calculation has been done

for the infinitely-wide two slab geometry,¹¹ and since the dispersion relation for that geometry is of the same form as the dispersion relation for the rectangular geometry, the same derivation may be used. (The difference between the two dispersion relations lies in the difference of the wavenumbers, s and q .) The result obtained for this dispersion relation is given below:

$$\Delta\omega_i^3 = \left[\frac{\sqrt{3} \omega_p^2 c}{4 \gamma^3 \beta k} \right]$$

$$\left[\frac{1 + \frac{a}{b} \frac{sb}{\epsilon} \frac{\tan(sb)}{\cosh^2(qa)}}{b^2 \left[\frac{\epsilon}{(sb)^2} + \frac{a^2}{b^2} \frac{1}{(qa)^2} + \left[\frac{\epsilon}{(sb) \tan(sb) \cos^2(sb)} \right] - \left[\frac{a^2}{b^2} \frac{\operatorname{sech}^2(qa)}{\tanh(qa)} \right] \right]} \right]$$

where ω_p^2 = the plasma frequency, which = $4\pi n_0 e^2/m$, and where n_0 = beam density, and the other terms are the same as defined for the single-particle calculation.

If we note that $I_b = nevA_b$, (A_b = beam area), we find that:

$$\omega_p^2 = \frac{4\pi c^2}{\beta} \frac{I_b}{I_0 A_b}$$

Finally, from page 38, we recall the expression for the effective beam current density, and note that this must be substituted for I_b into the above expression for ω_p^2 .

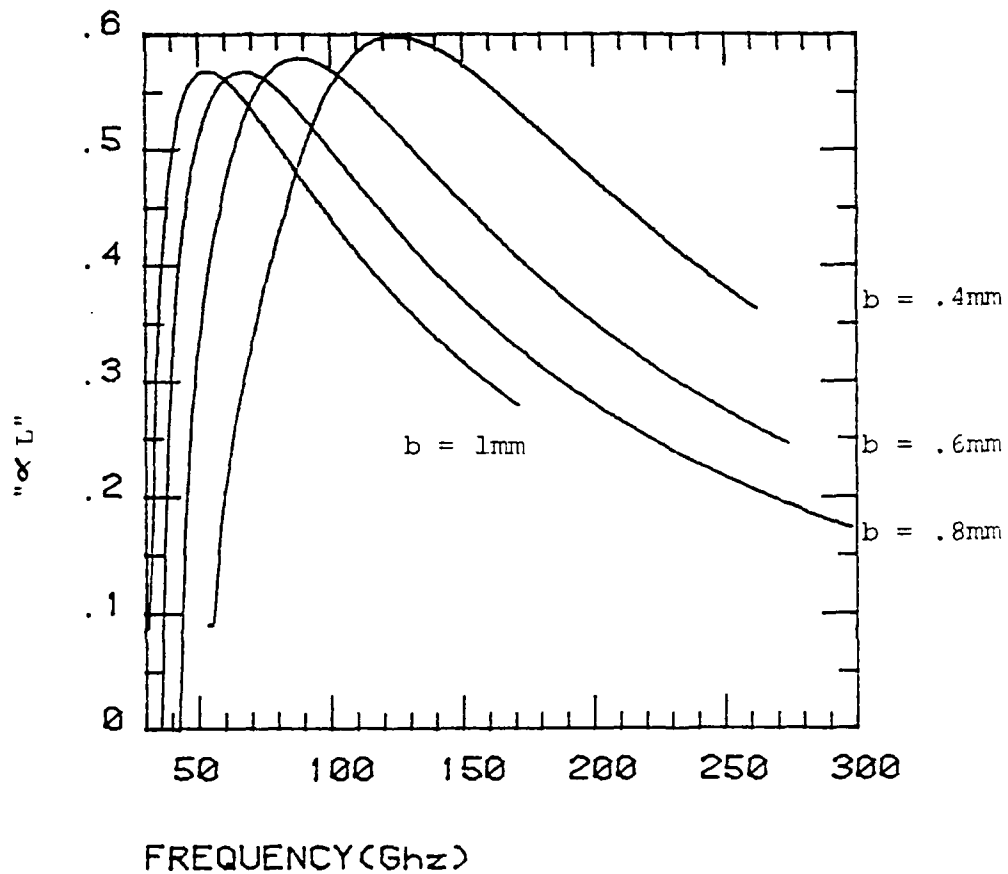
Collective Growth per Pass

As noted in Chapter 2, $\Delta\omega_i$ is the imaginary frequency shift due to the presence of the beam. Thus the energy in the wave will grow with an $e^{2\Delta\omega_i t}$ dependence. As in the single-particle calculation we can relate this temporal growth to the growth per pass, which gives

$$\alpha L = \frac{2\Delta\omega_i kL}{\omega}$$

Also, just as in the single-particle calculation, the above expression has a factor in it dependent on I_b and L , specifically, $L(I_b/I_0)^{1/3}$. Thus the plots in Figs. 4-5 - 4-7 show αL divided by this length-current term. It is clear from the plots that roughly the same output frequencies and bandwidths are predicted by the collective calculation as were predicted by the single-particle calculation.

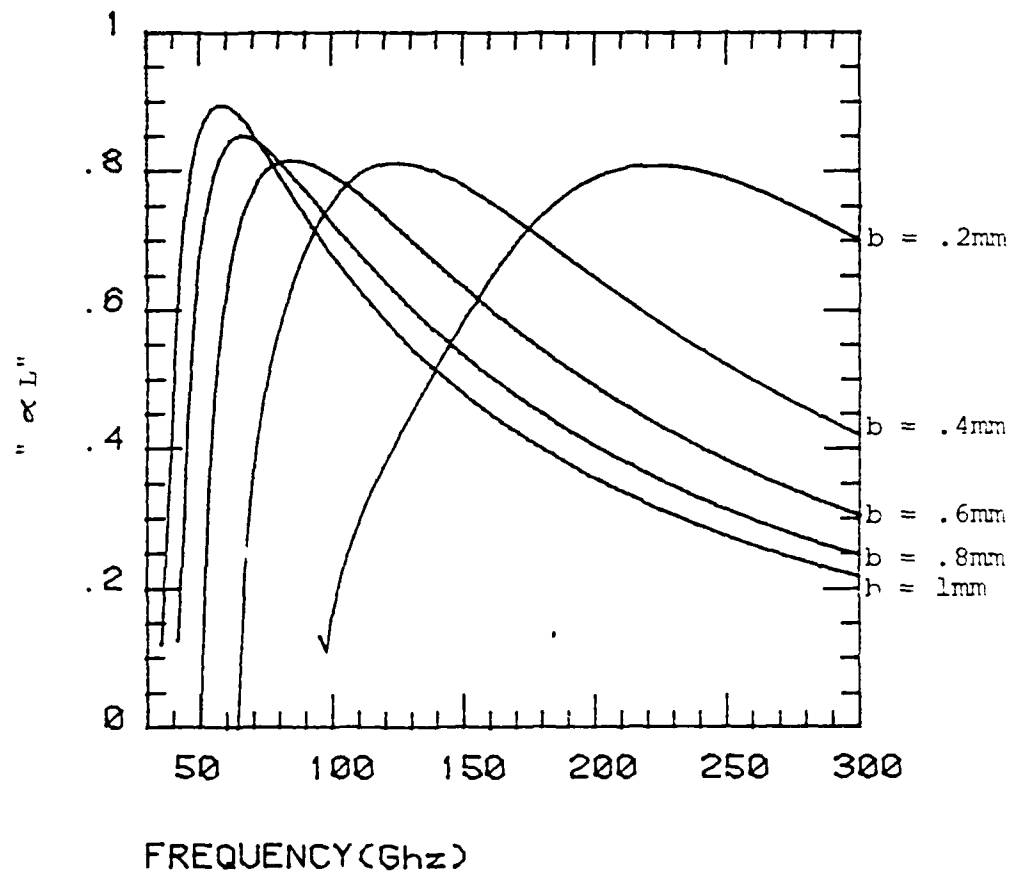
"ALPHA * L" vs. FREQUENCY(Ghz)



$$"\alpha L" = \frac{\alpha L}{\frac{LI_b}{I_0}}, I_0 = 17000 \text{ amps.}$$

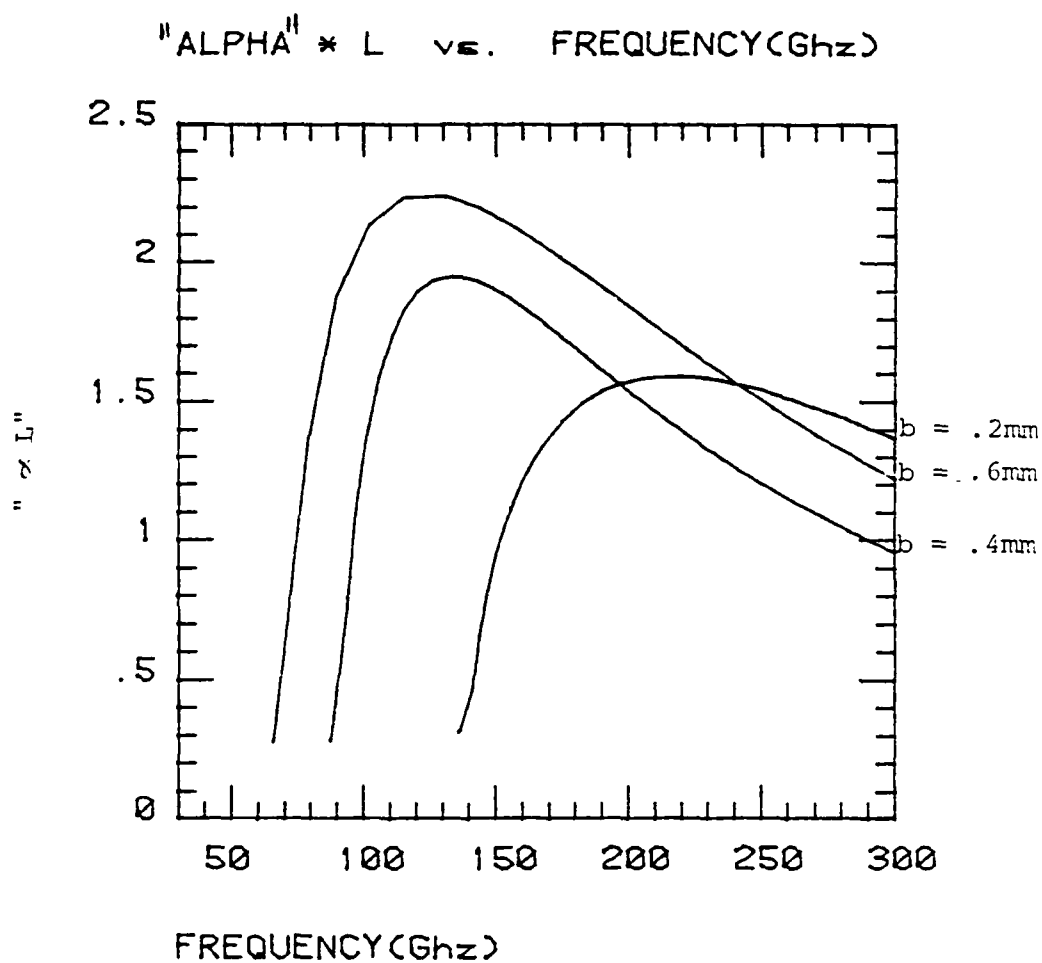
Fig. 4-5. Collective $\alpha L / L(I_b/I_0)^{1/3}$, for WR-42 size resonator. (b = dielectric slab thickness).

"ALPHA * L" vs. FREQUENCY (Ghz)



$$\alpha L = \frac{\alpha L}{\frac{L I_b}{I_0}}, \quad I_0 = 17000 \text{ amps.}$$

Fig. 4-6. Collective $\alpha L / L (I_b / I_0)^{1/3}$, for WR-28 size resonator. (b = dielectric-slab thickness).



$$"\alpha L" = \frac{\alpha L}{\frac{L I_b}{I_o}}, \quad I_o = 17000 \text{ amps.}$$

Fig. 4-7. Collective $\alpha L / L(I_b/I_o)^{1/3}$, for WR-12 size resonator. (b = dielectric-slab thickness).

Collective Growth Calculation Approximations

Several approximations were made in obtaining the above results:

--First, it was assumed that $\Delta\omega/\omega \ll 1$, so that the Taylor-series expansion is valid. We will test this assumption with practical current and resonator parameters in Chapter 5.

--Second, an approximation of $\tanh(u) = u$ was made,¹² the validity of which requires that

$$\frac{1}{2} \frac{\omega_p^2}{\gamma^3 (\Delta\omega)^2} < 1$$

This approximation will be questionable for high-density, low voltage beams. With our definition for ω_p^2 it becomes:

$$\frac{I_b}{A_b} < \left[\frac{(\Delta\omega)^2}{c^2} \right] \left[\frac{\beta \gamma^3}{2\pi} \right] I_0$$

Again, we defer applying this requirement to calculated results until Chapter 5.

--Finally, an approximation was made in using the infinite slab result at all for the rectangular geometry. This required that B_z for the LSM mode approach zero, so that the

mode could be approximated by a pure TM mode. The validity of this approximation is checked by plotting the energy contained in the B_z -component of the field, over the total energy in the fields. This plot is given in Fig. 4-8. We see that the B_z -component of the LSM mode is indeed quite small, with a maximum value of about 9%, so that use of the TM-mode growth-rate calculation should be a good approximation.

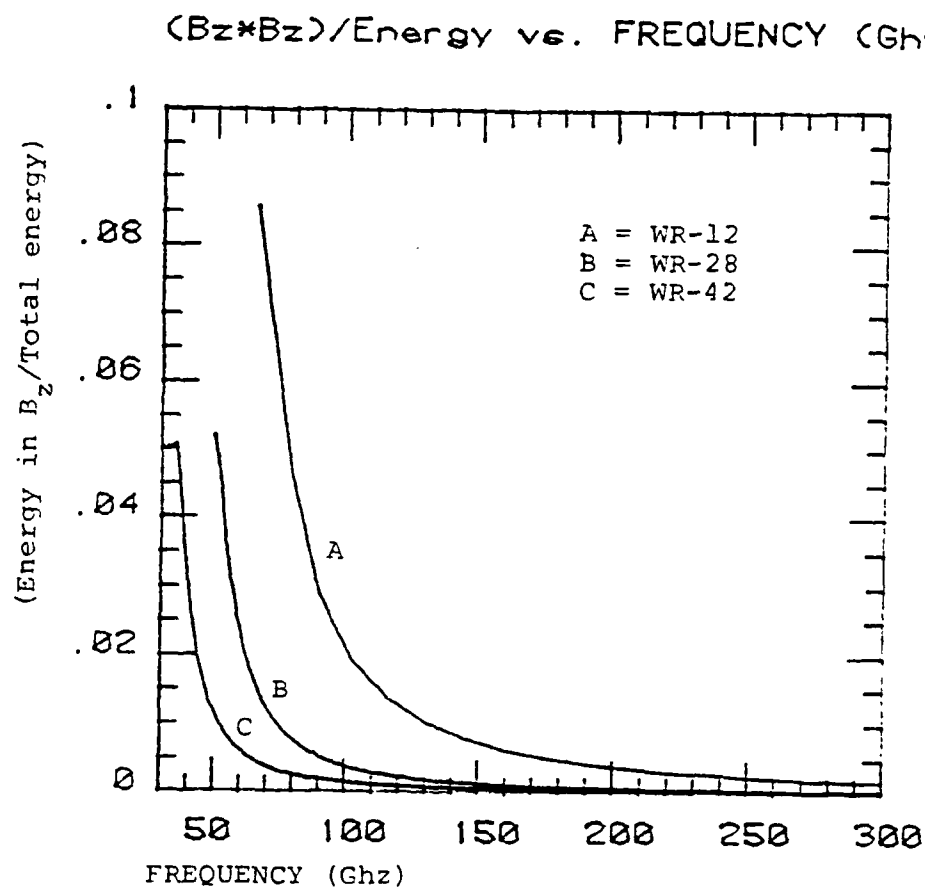


Fig. 4-8. $(\text{Energy stored in z-component of Magnetic field}) / (\text{Total Energy})$, for WR-42, WR-28, and WR-12 waveguide sizes. Dielectric-slab thickness = .6mm.

Chapter 5: The Dartmouth Cerenkov FEL as an High Power Amplifier

In this chapter we will complete the specialization, begun in Chapter 3, of our parameters to match those of the Dartmouth FEL. The purpose of this chapter is two-fold. First we want to see if the Dartmouth FEL, using the rectangular geometry, could operate as a high-gain, high-frequency amplifier; and, second, we wish to check that any approximations that we use will be valid for these real experimental parameters.

Use of Collective Calculation

We must first determine which of the two growth calculations, the collective or the single-particle calculation, should in general be used for high-gain applications. Note that the difference between the two calculations lay primarily in the assumed magnitudes of the gain. The single-particle calculation assumes that the fields are constant while the electrons do work on them. Thus it requires a gain per pass small enough so that the fields can be approximated to be constant during a transit time of an electron in the electron beam. We see immediately that for high-power amplification, which requires a gain per pass of at least $e^{\alpha L} = 10$, that this constant-field approximation must fail. Thus we are left

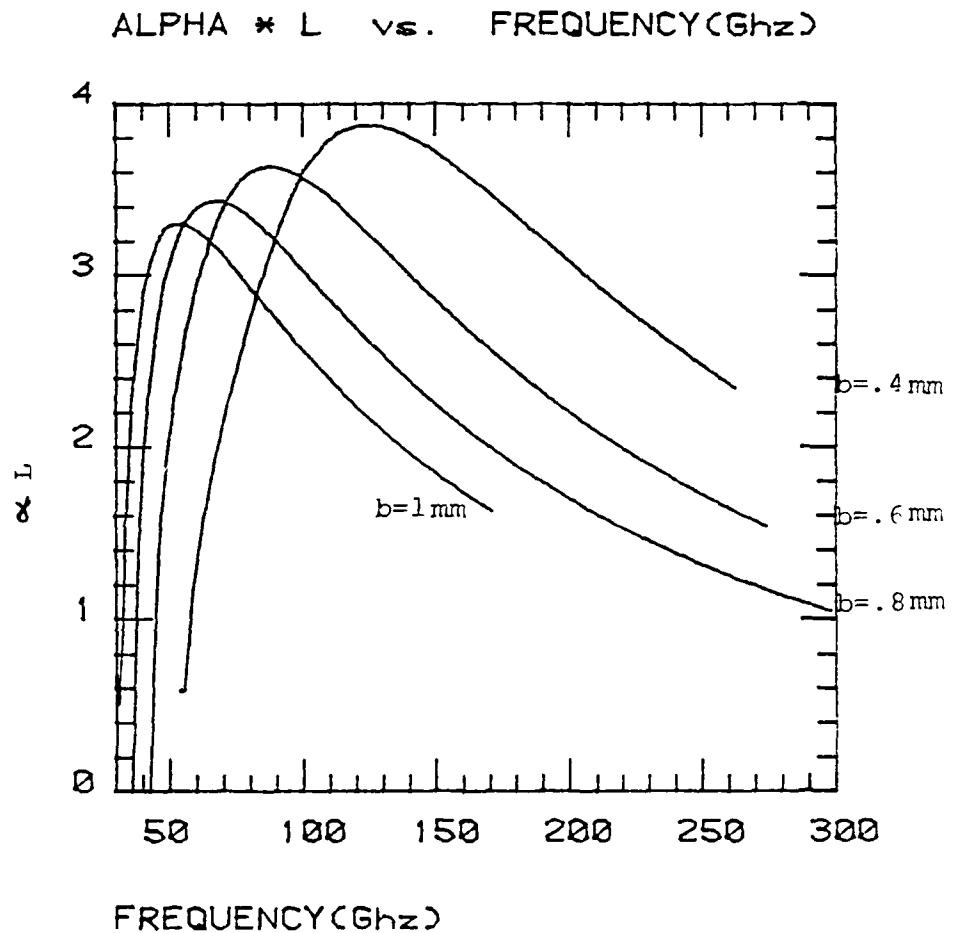
with the collective calculation for any high-gain application. Again note that the collective calculation requires that $\Delta\omega/\omega \ll 1$, but assumes nothing about the total gain per pass.

Parameters

We have already limited ourselves to the commercial waveguide sizes, and to operating voltages of less than 300 KV, to accomodate ourselves to the Dartmouth FEL. Thus we need only specify current density and resonator length to get parameters that will be completely applicable to that device. We choose a current density of 10 amps/cm², which is just within the capability of the Dartmouth device, and we choose a reasonable resonator length of 10cm.

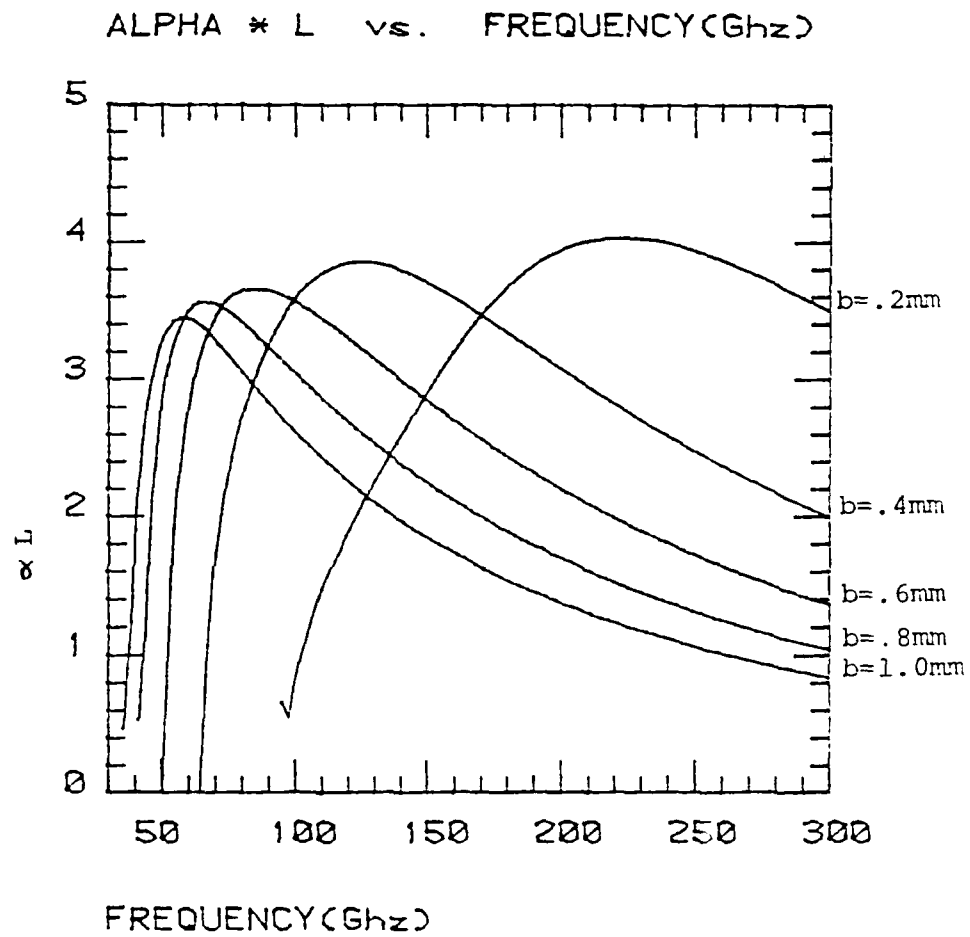
Results

We now plot αL vs. frequency for each of the waveguide sizes, and refer the reader to Fig. 3-7, 8, & 9 for the corresponding operating voltage information. (Fig. 5-1 - 5-3). Note that for each of the waveguide sizes, αL falls between 3 and 4, which means that the gain per pass, $e^{\alpha L}$, will be approximately 20 to 50. (In terminology more commonly used for amplifiers, this corresponds to gain per pass of 13 to 17 db). As mentioned earlier, for useful operation as a high-power amplifier, gain per pass of 10 (= 10 db) is necessary. Thus we are fairly well above this



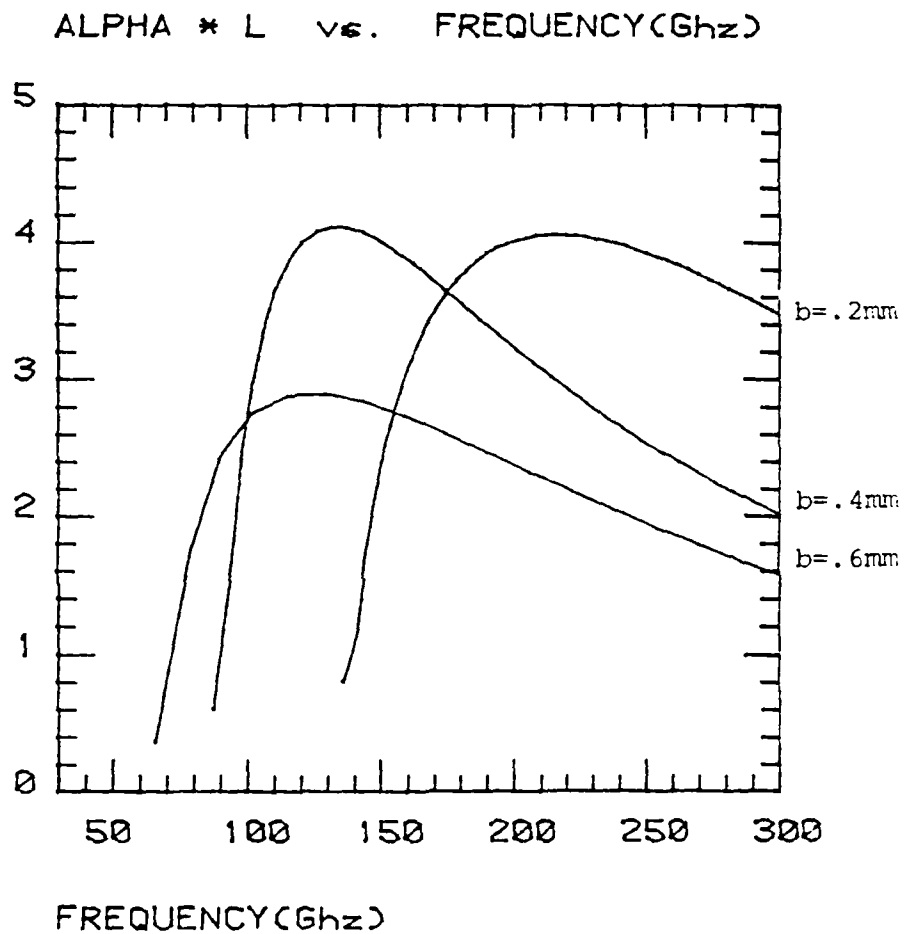
$$\frac{I_b}{A_b} = 10 \text{ amps/cm}^2, \quad L = 10 \text{ cm}$$

Fig. 5-1. αL vs. frequency for WR-42 size resonator, with current density = 10 amps/cm^2 , and resonator length = 10 cm . (b = dielectric-slab thickness)



$$\frac{I_b}{A_b} = 10 \text{ amps/cm}^2, \quad L = 10 \text{ cm}$$

Fig. 5-2. αL vs. frequency for WR-28 size resonator, with current density = 10 amps/cm^2 , and resonator length = 10cm. (b = dielectric-slab thickness)



$$\frac{I_b}{A_b} = 10 \text{ amps/cm}^2, \quad L = 10\text{cm}$$

Fig. 5-3. αL vs frequency for WR-12 size resonator, with current density = 10 amps/cm², and resonator length = 10cm, (b = dielectric-slab thickness)

requirement. (Note however, that losses in the dielectric and the conducting walls of the resonator will lower this performance, though certainly not below the required 10db.) Finally we note that peak gains at frequencies up to 200 Ghz are possible with the thinner dielectric slabs and the smaller waveguide sizes. Thus we may conclude that the 2-slab, rectangular resonator, using these parameters which correspond to those available from the Dartmouth FEL, should operate effectively as a high-power, high-frequency amplifier.

Now we need only to check the validity of the two assumptions that were made in the collective calculation.

The two assumptions that must hold are:

$$1. \frac{\Delta\omega}{\omega} \ll 1, \text{ and}$$

$$2. \frac{I_b}{A_b I_0 (\Delta\omega/c)^2} \frac{2\pi}{\beta\gamma^3} < 1$$

Calculating peak $\Delta\omega_i$'s from the plots of αL gives that $\Delta\omega/\omega$ ranges from .03 to .01, which is certainly $\ll 1$. Doing a similar calculation for the second expression gives

$$\frac{I_b}{A_b I_0} \frac{2\pi}{(\Delta\omega/c^2)} \frac{1}{\beta\gamma^3} \approx .2$$

Thus we see that both these assumptions do hold for these particular parameters and results.

Conclusions

We have seen generally that the rectangular, 2-slab resonator for a Cerenkov FEL does show promise for use as a high-power amplifier at frequencies up to 300 Ghz. Even for the relatively low current, low voltage FEL at Dartmouth, gains per pass greater than 10db, at frequencies of up to 200 Ghz should be achievable. The obvious next step must be an experimental verification of these results.

Appendix 1: Derivation of Dispersion Relations for LSE and LSM Modes

Maxwell's equations:

$$\nabla \cdot \mathbf{D} = 4\pi\rho$$

$$\nabla \cdot \mathbf{B} = 0$$

$$\nabla \times \mathbf{E} = -\frac{1}{c} \frac{\partial \mathbf{B}}{\partial t}$$

$$\nabla \times \mathbf{H} = \frac{4\pi \mathbf{J}}{c} + \frac{1}{c} \frac{\partial \mathbf{D}}{\partial t}$$

if reduced to component form, yield eight equations relating the different field components to one another.¹³ We immediately assume a time- and z-dependence of $e^{i(kz - \omega t)}$, with propagation in the z-direction, and further assume that there are no sources present. Then the x- and y-component equations of Maxwell's curl equations can be reduced to the following form, with all transverse field components in terms of the z-field components:

$$E_y = \frac{i}{p^2} \left[k \frac{\partial E_z}{\partial y} - \frac{\omega}{c} \frac{\partial B_z}{\partial x} \right]$$

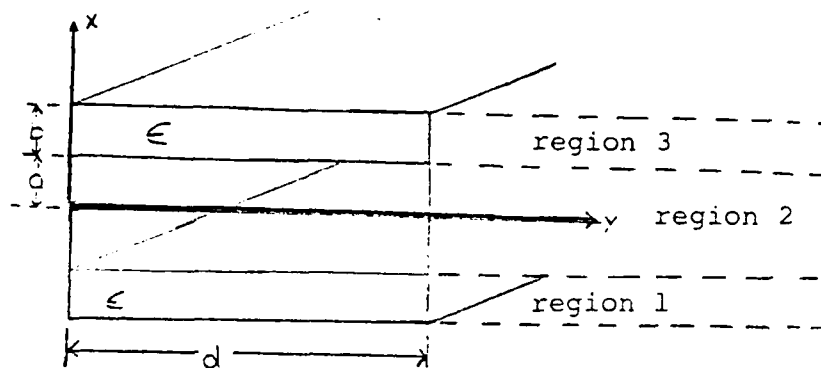
$$E_x = \frac{i}{p^2} \left[k \frac{\partial E_z}{\partial x} + \frac{\omega}{c} \frac{\partial B_z}{\partial y} \right]$$

$$B_y = \frac{i}{p^2} \left[k \frac{\partial B_z}{\partial y} + \frac{\omega \epsilon}{c} \frac{\partial E_z}{\partial x} \right]$$

$$B_x = \frac{i}{p^2} \left[k \frac{\partial B_z}{\partial x} - \frac{\omega \epsilon}{c} \frac{\partial E_z}{\partial y} \right]$$

where: $p^2 = \frac{\omega^2 \epsilon}{c^2} - k^2$

We now apply these equations to the following geometry:



If we assume that this geometry has infinitely conducting walls, the following boundary conditions on the fields must hold:

$$E_{\text{tan}} = 0 \text{ on conductors} \text{-----} E_z, E_y = 0 \text{ at } x = \pm(a+b)$$

$$E_z, E_x = 0 \text{ at } y = 0, d$$

$$E_{\text{tan}} \text{ continuous} \text{-----} E_z, E_y \text{ continuous at } x = \pm a$$

$$D_{\text{nor}} \text{ continuous} \text{-----} D_x \text{ continuous at } x = \pm a$$

All B-components are continuous at $x = \pm a$.

It can be shown ⁹ that this geometry will support two mode-types: LSE, (for which $E_x = 0$), and LSM, (for which B_x

= 0). Thus, from the transverse-component form of Maxwell's Equations given above, we have the following relations between E_z and B_z for each of the mode-types.

LSE:

$$\frac{k \partial E_z}{\partial x} = - \frac{\omega}{c} \frac{\partial B_z}{\partial y}$$

LSM:

$$\frac{k \partial B_z}{\partial x} = \frac{\omega \epsilon}{c} \frac{\partial E_z}{\partial y}$$

Geometry of Fields

In order to actually calculate the fields, we initially assume that all field components will be made up of some combination of trigonometric functions, of the general form:

$$[A \sin(sx) + B \cos(sx)][C \sin(ty) + D \cos(ty)]$$

We next apply the boundary conditions on the conducting surfaces to this general form, and find that to satisfy these conditions E_z must be of the form:

$$E_z = A \sin(ty) [B \sin(sx) + C \cos(sx)]$$

$$\text{with } t = \frac{n}{d}, \quad n = 1, 2, 3, \dots$$

We now can use the transverse-field Maxwell's Equations to get the rest of the field components. First, however, we must address the fact that we have 3 regions in the resonator. Obviously regions 1 and 3 must be identical. They will however, differ from region 2 in that they will have different wavenumbers (due to the difference in dielectric constant.) Therefore, we let s be the wave-number in the slab regions (1 & 3), and let r = wave-number in the vacuum region, (Region 2). We now make one final assumption before actually finding the fields. We assume that the fields are symmetric about $x = 0$. We do this because we will eventually want to couple the fields to an electron beam traveling in the vacuum region of the resonator. Thus, to get maximum coupling between the resonator fields and the beam, the fields must be as strong as possible in the that region. Note, however, that fields asymmetric about $x = 0$ must equal 0 at $x = 0$, while symmetric fields will never equal zero in the vacuum region. The symmetric fields will, therefore, couple more strongly to the beam than will asymmetric fields. Thus we consider only the symmetric fields here, which simply means that we use only $\cos(x)$ terms in the expressions for the fields in the vacuum region. Thus the following fields for each of the modes in each of the 3 regions of the resonator are found.

LSE MODES

Region 1:

$$E_z = A \sin(ty) [\sin(sx) + \tan[s(a+b)] \cos(sx)]$$

$$E_y = (ik/t) A \sin(ty) [\sin(sx) + \tan[s(a+b)] \cos(sx)]$$

$$B_z = \frac{ks}{(\omega/c)t} A \cos(ty) [\cos(sx) - \tan[s(a+b)] \sin(sx)]$$

$$B_x = \frac{i(s^2 - \omega^2 \epsilon/c^2)}{t(\omega/c)} A \cos(ty) [\sin(sx) + \tan[s(a+b)] \cos(sx)]$$

$$B_y = \frac{is}{(\omega/c)} A \sin(ty) [\cos(sx) - \tan[s(a+b)] \sin(sx)]$$

$$\text{where } A = E_{z0} \frac{[1 - \tan(sa)\tan(sb)]}{\sec(sa)\tan(sb)},$$

and E_{z0} = the magnitude of E_z at the center
of the dielectric interface.

Region 2:

$$E_z = F \sin(ty) \cos(rx)$$

$$E_y = (ik/t) F \cos(ty) \cos(rx)$$

$$B_x = \frac{-i[-r^2 + (\omega^2/c^2)]}{(\omega/c)t} F \cos(ty) \cos(rx)$$

$$B_y = \frac{-i r}{(\omega/c)} F \sin(ty) \sin(rx)$$

$$B_z = \frac{-kr}{(\omega/c)t} F \cos(ty) \sin(rx)$$

where $F = E_{z0}/\cos(ra)$.

Finally,

Region 3 = Region 1

LSM MODES

Region 1:

E_z = same as for LSE-mode.

$$E_y = (-it/k) A \cos(ty) [\sin(sx) + \tan[s(a+b)] \cos(sx)]$$

$$E_x = \frac{(k^2 + t^2)}{ks} A \sin(ty) [\cos(sx) - \tan[s(a+b)] \sin(sx)]$$

$$B_y = \frac{i(\omega\epsilon/c)}{s} A \sin(ty) [\cos(sx) - \tan[s(a+b)] \sin(sx)]$$

$$B_z = \frac{(\omega\epsilon/c)t}{ks} A \cos(ty) [-\cos(sx) + \tan[s(a+b)] \sin(sx)]$$

Region 2:

E_z = same as for LSE-mode.

$$E_y = (-it/k) F \cos(rx) \cos(ty)$$

$$E_x = \frac{i(k^2 + t^2)}{kr} F \sin(ty) \sin(rx)$$

$$B_y = \frac{i(\omega/c)}{r} F \sin(ty) \sin(rx)$$

$$B_z = \frac{(\omega/c)t}{kr} F \cos(ty) \sin(rx)$$

and again,

Region 3 = Region 1

Now we must be sure that the rest of Maxwell's equations, namely the divergence equations and the relation given by the z-component of the curl equations, are satisfied. These give the following requirements on the wave numbers:

$$r^2 = \frac{\omega^2}{c^2} - k^2 - t^2 ;$$

$$s^2 = \frac{\omega^2 \epsilon}{c^2} - k^2 - t^2$$

Now note that for operation of a Cerenkov FEL, the waves must be slow waves, so that $k > \omega/c$. This, however, makes $r^2 < 0$. Therefore we let

$$q^2 = -r^2, \quad q = ir$$

so that all trigonometric functions of r become hyperbolic functions of q .

As a final step we apply the rest of the boundary conditions, the continuity conditions at the dielectric interfaces, to these field components, and so obtain the dispersion relations for the two mode types. This rather tedious calculation yields finally:

$$\text{LSM: } \frac{\tanh(qa)}{qa} = \frac{\epsilon b}{a} (sb) \cot(sb)$$

$$\text{LSE: } -(qa) \tanh(qa) = \frac{a}{b} (sb) \cot(sb)$$

Appendix 2: Calculation of n/n_0

The initial equation for n is

$$n = \frac{\int dA n |E_z|^2}{|E_{z0}|^2 A_b}$$

where A_b is the beam area, which equals $2ad$ (see page 63), and where n is the beam density.

We assume that $n = n_0$, a constant over the area of the beam, and we assume that the beam is a distance h away from the dielectric surface. From appendix 1 we get that:

$$E_{z_{LSM}} = \frac{E_{z0} \sin(ty) \cosh(qx)}{\cosh(qa)}$$

Thus we have:

$$n = \frac{n_0}{(2ad) 4 \cosh^2(qa)} \int_0^d dy \int_{-(a-h)}^{a-h} \sin^2(ty) \cosh^2(qx) dx$$

Therefore:

$$\frac{n}{n_0} = \frac{1}{4 \cosh^2(qa)} \left[\frac{\sinh[2q(a-h)]}{2q(a-h)} + 1 \right]$$

Appendix 3: Calculation of the Total Energy
in Fields for LSE and LSM modes.

The total energy in an electromagnetic field is given by¹⁴:

$$\mathcal{E} = \frac{1}{16\pi} \int_V \vec{E} \cdot \vec{D}^* + \vec{B} \cdot \vec{H}^* dV = W_e + W_m.$$

This quantity could be computed directly from the fields given in appendix 1, but if we first note the $W_e = W_m$, we can greatly shorten the calculation. For the LSE mode (with $E_x = 0$), we have:

$$\mathcal{E} = 2W_e = \frac{1}{8\pi} \int_V |E_y|^2 + |E_z|^2 dV$$

and similarly for the LSM mode (with $B_x = 0$)

$$\mathcal{E} = 2W_m = \frac{1}{8\pi} \int_V |B_y|^2 + |B_z|^2 dV$$

Now for the rectangular geometry described in this paper (see Fig. 3-1), these integrals become:

$$\int_V dV = \int_0^L dz \int_0^d dy \left[2 \int_a^{a+b} dx + \int_{-a}^a dx \right]$$

\uparrow
region 1

\uparrow
region 2

where the appropriate fields, corresponding to the appropriate regions (vacuum and dielectric) must be used in

the x-integration. These integrals are then done for each of the modes, using the field components found in appendix 1. The results are cumbersome, but if we use the following identities, obtained by doing the integrals and then simplifying the results using simple trigonometric identities, the final results can be reduced to those given in chapter 4.

$$\int_a^{a+b} [\sin(sx) - \tan[s(a+b)] \cos(sx)]^2 dx =$$

$$\frac{1}{\cos^2[s(a+b)]} \left[\frac{b}{2} - \frac{\sin(2sb)}{4s} \right]$$

$$\int_a^{a+b} [\cos(sx) + \tan[s(a+b)] \sin(sx)]^2 dx =$$

$$\frac{1}{\cos^2[s(a+b)]} \left[\frac{b}{2} + \frac{\sin(2sb)}{4s} \right]$$

References

1. K.L. Felch, Cerenkov Radiation in Dielectrically-loaded Waveguides; Ph.d. thesis, (1980). Dartmouth College Physics Department. p. 7.
2. Ibid., p. 46.
3. Ibid., p. 56.
4. Ibid., p. 106.
5. J.E. Walsh, "Stimulated Cerenkov Radiation"; in Advances in Electronics and Electron Physics, (Vol. 58). Academic Press, New York, (1982). p. 306.
6. J.R. Pierce, Traveling-Wave-Tubes. Von Nostrand Company, (1950). p. 16.
7. J.E. Walsh & J.B. Murphy, "Tunable Cerenkov Lasers"; in IEEE Journal of Quantum Electronics, Vol. QE-18, No. 8, August 1982.
8. Felch, Chapter 3.
9. R.E. Collin, Field Theory of Guided Waves. McGraw Hill, (1960). Chapter 6.
10. J.E. Walsh. Private Communication.
11. Felch, p. 117.

12. Felch, p. 125.
13. R.E. Collin, Foundations of Microwave Engineering.
McGraw Hill, New York, 1966. p. 66.
14. J.D. Jackson, Classical Electrodynamics. John Wiley
& Sons, New York, 1975. p. 242.

**ATE
LMED**